Utjecaj poroznosti na mehaničko ponašanje staklenim vlaknima ojačane PBT smole

Perić, Marko

UNIVERSITY OF ZAGREB
FACULTY OF MECHANICAL ENGINEERING AND NAVAL ARCHITECTURE

MASTER'S THESIS

Marko Perić

Zagreb,2019.

UNIVERSITY OF ZAGREB
FACULTY OF MECHANICAL ENGINEERING AND NAVAL ARCHITECTURE

MASTER'S THESIS

Influence of Porosity on the Mechanical Behavior of Glass Fibre-Reinforced PBT Resin

Mentor:

Prof. dr.sc. Zdenko Tonković,

Student:

Marko Perić

Zagreb, 2019.

IZJAVA

Pod punom moralnom odgovornošću izjavljujem da sam ovaj rad izradio samostalno, koristeći se znanjem stečenim za vrijeme studija te navedenom literaturom.

STATEMENT

Under fully moral responsibility I declare that the thesis is entirely the result of my work and based on knowledge acquired during my studies and the literature cited.

ACKNOWLEDGMENT

I would like to thank my mentor, Professor Zdenko Tonković, for the opportunity he has given me, and all the advice and assistance he has given in the development of this work. In addition to Professor Tonković, I also thank Tomislav Lesičar, Ph.D., who, with his time, tips and ideas, contributed greatly to the development of this work. Big thanks also to Mr. Ante Bubalo from Yazaki Europe LTD, for the opportunity to cooperate and all the experiments he has carried out as part of this work.

Finally, a special thanks to my family, for the unconditional support throughout my years of study, and to all my friends and colleagues.

Marko Perić

SVEUČILIŠTE U ZAGREBU
FAKULTET STROJARSTVA I BRODOGRADNJE
Središnje povjerenstvo za završne i diplomske ispite
Povjerenstvo za diplomske ispite studija strojarstva za smjerove:
procesno-energetski, konstrukcijski, brodostrojarski i inženjersko modeliranje i računalne simulacije

Sveučilište u Zagrebu Fakultet strojarstva i brodogradnje	
Datum	Prilog
Klasa:	
Ur. broj:	

DIPLOMSKI ZADATAK

Student: **Marko Perić** Mat. br.: 0035196638

Naslov rada na hrvatskom jeziku: **Utjecaj poroznosti na mehaničko ponašanje staklenim vlaknima ojačane PBT smole**

Naslov rada na engleskom jeziku: **Influence of Porosity on the Mechanical Behaviour of Glass Fibre-Reinforced PBT Resin**

Opis zadatka:

Yazaki Corporation develops and produces specialized automotive connectors and terminals. A connector housing for an automobile in which wire harnesses and terminal fittings are incorporated, is injection-moulded of a resin. Due to its excellent mechanical and electrical properties as well as heat and water resistance Polybutylene terephthalate (PBT) is often used as the moulding material of the connector housing. In order to reduce the size and thickness of the connector housings, fibres such as glass fibres are added to the PBT to increase the strength of the housing. However, during the injection process of the component, defects such as porosities can appear inside PBT, degrading the strength and quality of the product.

The objective of this master thesis will be to investigate the influence of porosity on the homogenized response of the glass fibre-reinforced PBT and strength of the connector housing. Based on everything said above in this study it is necessary to:

1. Study available literature on the modelling of anisotropic material behaviour and on the homogenization methods for the estimation of effective mechanical properties of heterogeneous materials.
2. Determine the necessary 2D and 3D representative volume element size and geometry of a glass fibre-reinforced PBT consisting of various porosity ratio using appropriate boundary conditions.
3. Estimate the effective response of a reinforced PBT consisting of various porosity ratio using homogenization methodology.
4. If possible, validate the numerical results by comparison with the experimental measurements.

During thesis preparation one must comply with the standard rules for preparation of master thesis. It is necessary to list all literature used and received assistance.

Zadatak zadan: 26. rujna 2019.

Datum predaje rada: 28. studenoga 2019.

Predviđeni datum obrane: 2. – 6. prosinca 2019.

Zadatak zadao:

Prof. dr. sc. Zdenko Tonković

Predsjednica Povjerenstva:

Prof. dr. sc. Tanja Jurčević Lulić

CONTENTS

LIST OF FIGURES

LIST OF TABLES

LIST OF SYMBOLS AND UNITS

Latin symbols

Symbol	Unit	Description
n	-	Outward unit normal to $\partial\omega$
u	mm	Displacement in x direction
u	mm	Displacement
v_0	-	Volume fraction of first phase
v_1	-	Volume fraction of second phase
w	mm	Displacement in z direction
$\mathbf{x}$	-	Micro point
$\mathbf{A}^{\varepsilon}$	-	First strain concentration tensor
$\mathbf{B}^{\varepsilon}$	-	Second strain concentration tensor
$\mathbf{C}$	-	Elastic matrix
$\overline{\mathbf{C}}$	-	Macro stiffness
$\mathbf{C}_0$	(kgm/s^2)/m^2	Uniform stiffness
$\mathbf{E}$	-	Macro strain
$\mathbf{H}^{\varepsilon}$	-	Single Inclusion strain concentration tensor
$\mathbf{N}$	-	Shape function
$\mathbf{P}^{\varepsilon}$	-	Hill's polarization tensor
$\mathbf{X}$	-	Macro point
D	mm	Diameter
E	MPa	Youngs's Modulus
F	N	Force
I	mm^3	Ellipsoidal Volume
L	mm	Length
V	mm^3	Volume

Greek symbols	**Unit**	**Description**
Symbol	MPa	Macro stress
ε_{11}	-	Uniaxial peak strain
$\langle \varepsilon_{ij} \rangle$	-	Average strain
ε^*	-	eigenstrain
ξ	-	Eshelby's tensor
ξ	-	Natural coordinate
η	-	Natural coordinate
σ	MPa	Macro stress
$\langle \sigma_{ij} \rangle$	MPa	Average stress
v	-	Poisson's ratio
ω	-	domain

LIST OF ABBREVIATIONS

Abbreviation	Description
1D	One dimensional
2D	Two dimensional
3D	Three dimensional
BC	Boundary conditions
CAE	Computer Aided Engineering
CCD	Charge coupled device
CPU	Central processing unit
CT	Computer Tomography
D-I	Double Inclusion problem
DIC	Digital Image Correlation
EDS	Electronic distribution systems
EIP	Equivalent inclusion problem
FE	Finite element
FEA	Finite element analysis
FEM	Finite element method
GF	Glass fiber
GFRP	Glass fiber reinforced polymers
HC	Hydrocerol
MF	Mean-field
MFH	Mean-field homogenization
MMC	Metal matrix composites
MT	Mori-Tanaka
NDT	Nondestructive testing
PBT	Polybutylene terephthalate
PET	Polyethylene terephthalate
RMC	Rubber matrix composites
RVE	Representative volume element
S-C	Self-consistent problem

SAŽETAK (Abstract in Croatian)

Ovaj diplomski rad je napravljen u suradnji Yazaki Europe Ltd. Yazaki je jedna od svjetskih proizvođača električnih komponenata za automobilsku industriju. Između ostalog bave se proizvodnjom, razvojem i istraživanjem električnih distributivnih sistema (EDS), elektroničnih komponenata i instrumenata, konektora i terminala. Na cijel skup proizvoda se postavljaju visoki zahtjevi koji uključuju dobre mehaničke i električne karakteristike, te otpornost na toplinu i tekućine. Rad je izrađen sa ciljem da se analizira jedan od problema koji se javlja kao posljedica injekcijskog prešanja komponenata kompleksnih geometrija. Materijal koji se analizira je heterogen i anizotropan te sastoji se od osnovnog PBT-a (Polibutilen tereftalat) i staklenih vlakana (GF) čiji udio može biti raznovrstan, no uzet će se vrijednost od 20%. S obzirom da se takva miješana talina ubrizgava u kalup koji je složene geometrije, zbog lošeg strujanja i struganja po površini kalupa, talina ne uspijeva kvalitetno ispuniti kalup i dolazi do pojavljivanja poroznosti. Poroznost za posljedicu ima smanjenje mehaničkih svojstava i cilj ovog rada je analizirati kakav je upravo taj utjecaj poroznosti. Staklena vlakna, u obliku štapića, koja se dodaju u osnovni PBT materijal su izrazito mala i njihovo modeliranje stvara određene probleme, kao što je nemogućnost definiranja realne geometrije i dimenzija. Pretpostavljeno je linearno ponašanje konstituenata i male deformacije.

Područje istraživanja ovog rada se može podijeliti u četiri cjeline:

1. Istražiti svojstva anizotropnih i heterogenih materijala te proučiti metode homogenizacije pomoću kojih ih je moguće opisati sa ciljem određivanja mehaničkih karakteristika.
2. Odrediti 2D i 3D reprezentativne volumenske elemente (RVE) materijala koji se sastoje od PBT-a i 20% staklenih vlakana i pronaći veličinu RVE-a pomoću kojega je moguće na mikro razini opisati mehaničko ponašanje materijala na makro razini.
3. Uz PBT i 20% staklenih vlakana, modelirati reprezentativne volumenske elemente (RVE) sa udjelom pora.
4. Dobivene numeričke rezultate usporediti sa vrijednostima dobivenima eksperimentom.

U prvom i drugom poglavlju su opisana heterogena i anizotropna svojstva materijala. Materijal koji se proučava je heterogen jer se sastoji od osnovne faze, Polibutilen tereftalata i uključina u obliku staklenih vlakana, a orijentacije vlakana je raznovrsna te se može reći da je materijal i

anizotropan. Također je proučena metoda homogenizacije heterogenih materijala, od kojih je posebno izdvojena Mori-Tanaka metoda.

U trećem poglavlju se pomoću programskog paketa *Digimat* provela analitička MF (Mean-field) homogenizacijska metoda i rezultati su se uspoređivali sa rezultatima proizvođača materijala.

U četvrtom poglavlju su se pomoću *Digimat*-a i *Abaqus*-a, generirale različite veličine 2D i 3D reprezentativnih volumenskih elemenata (RVE-a) materijala sa različitim orijentacijama staklenih vlakana. Razmatrale su se 3 različite orijentacije staklenih vlakana te 4 različite veličine RVE-a. Svi dobiveni rezultati su se uspoređivali sa σ - ε dijagramom i tražili su se oni modeli koji dobro opisuju stvarno ponašanje materijala uz uvjet da daljnjim povećanjem RVE-a ne dolazi do značajne promjene u dobivenim rezultatima. Razmatrala se periodična geometrija sa nametnutim periodičnim opterećenjem i rubnim uvjetima.

U petom poglavlju je bio cilj provesti analizu modela iz prethodnog poglavalja no uz dodatak pora u materijalu. Odabran je RVE određene veličine i određene orijentacije vlakana iz razloga što se pokazalo da dobro opisuje stvarno ponašanje materijala te uz daljnje povećanje geometrije ne dolazi do značajnih promjena u rezultatu. S ciljem usporedbe dobivenih rezultata, proveo se eksperiment na testnom uzorku epruvete. Epruvete su dobivene postupkom injekcijskog prešanja uz poseban dodatak Hidrocerola čije prisustvo je omogućilo nastanak proznosti unutar strukture materijala. Kako bi se analiza i eksperiment što kvalitetnije usporedili, epruvete su posnimane CT metodom, te su dobivene vrijednosti volumnog udjela i prosječne veličine pora, koje su onda korištene u generiranju računalnih modela. Tlačni test na epruvetama je napravljen i rezultati dobiveni DIC (Digital Image Correlation) metodom su služili za usporedbu numeričkih rezultata sa eksperimentom.

Zadnje poglavlje sadrži zaključke provedenog istraživanja i njemu su dane upute za daljnji rad.

Ključne riječi: *polibutilen tereftalat, staklena vlakna, poroznost, Mori Tanaka metoda, homogenizacija, metoda konačnih elemenata, reprezentativni volumenski element (RVE), Abaqus, Digimat*

SUMMARY

This thesis is made in collaboration with Yazaki Europe Ltd. Yazaki is one of the world's manufacturers of electrical components for the automotive industry. Among other things, they are engaged in the production, development and research of electrical distribution systems (EDS), electronic components and instruments, connectors and terminals. The entire product set is subject to high requirements that include good mechanical and electrical performance, as well as resistance to heat and fluids. This thesis is made with goal to analyze one of the problems that occurs as a result of injection molding of components of complex geometries. The material to be analyzed is heterogeneous and anisotropic and consists of basic PBT (Polybutylene terephthalate) and glass fiber (GF) whose fraction may be varied, but 20% will be taken. Because such mixed melt is injected into a mold of extremely complex geometries, due to poor flow and scraping on the mold surface, the melt fails to fill the mold well and porosity occurs. Porosity results in a decrease in mechanical properties and the aim of this thesis is to analyze exactly what the effect of porosity is. Glass fibers in the form of sticks that are added to the basic PBT material are extremely small and their modeling creates certain problems, such as the inability to define realistic geometries and dimensions. The linear behavior of the constituents and the small deformations were assumed.

The research area of this thesis can be divided into four sections:

1. Investigate the properties of anisotropic and heterogeneous materials and study homogenization methods that can be used to determine mechanical properties.
2. Determine 2D and 3D representative volume elements (RVE) of materials consisting of PBT and 20% fiberglass and find the size of the RVE by which it is possible to describe at the micro level the mechanical behavior of the material at the macro level.
3. With PBT and 20% glass fiber, model representative volume elements (RVEs) with porosity
4. Validate numerical results by comparison with the experiment.

The first and second Chapter describe the heterogeneous and anisotropic properties of the material. The material under study is heterogeneous because it consists of the basic phase, polybutylene terephthalate and glass fiber inclusions, and the fiber orientation is varied and can be said that material is anisotropic. The method of homogenization of heterogeneous materials was also studied, of which the Mori-Tanaka method is singled out.

In Chapter three, an analytical MF (Mean-field) homogenization method was implemented using the *Digimat* software package and the results are compared with those of the material manufacturer.

In Chapter four, different sizes of 2D and 3D representative volume elements (RVEs) of materials with different glass fiber orientations are generated using *Digimat* and Abaqus. Three different orientations of glass fibers and four different sizes of RVE were considered. All the results obtained were compared with the σ-ε diagram and those models that required a good description of the actual behavior of the material were sought, provided that further increase in RVE did not lead to a significant change in the results obtained. Periodic geometry with imposed periodic loading and boundary conditions was considered.

In Chapter Five, the aim was to carry out an analysis of the models in the previous chapter but with the addition of pores in the material. A RVE of a certain size and a specific fiber orientation was selected for the reason that it was shown to describe well the actual behavior of the material and that with a further increase in geometry no significant changes in the result occurred. In order to compare the results obtained, an experiment was conducted on a test sample of the test tube. The tubes were obtained by injection molding with the special addition of Hydrocerol, the presence of which allowed the formation of a pores within the material structure. In order to better compare the analysis and the experiment, the tubes were imaged using the CT method, and the values of volume fraction and average pore size were obtained, which were then used in the generation of computer models. A tensile test on the tubes is made and the results obtained by the DIC (Digital Image Correlation) method were used to compare the numerical results with the experiment.

The last chapter contains the conclusions of the research conducted and is given directions for further work.

Key words: *polybutylene terephthalate, glass fibers, porosity, Mori Thin method, homogenization, finite element method, representative volume element (RVE), Abaqus, Digimat*

1 Introduction

This Master's thesis is written in collaboration with Yazaki Europe LTD from Zagreb. Yazaki is one of the world's leading manufacturers of electrical components for the automotive industry. Among other things, they are engaged in the production, development and research of electrical distribution systems (EDS), electronic components and instruments, connectors and terminals.

A common material used in making such enclosures is polybutylene terephthalate (PBT), because of its favorable material properties and high resistance to heat and water. "PBT belongs to group of (semi-) crystalline polymers, i.e. polyester thermoplastics. The preparation process is carried out by polymerization of butanediol and terephthalic acid. Structure of PBT is very similar to polyethylene terephthalate (PET) and they differ in the number of methylene (CH_2) groups present in the repeating units of polymer molecules."[1]. Its chemical structure is shown in Figure 1.1.

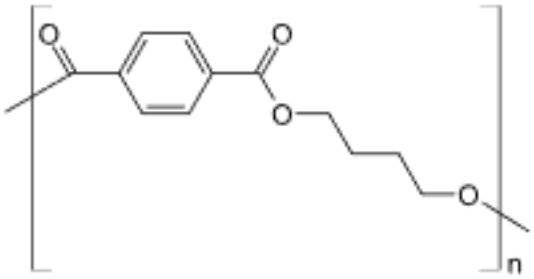

Figure 1.1 Chemical structure of polybutylene terephthalate [2]

In terms of mechanical properties, PBT is characterized by its high strength and stiffness in different atmospheric conditions. It is resistant to high temperatures and aging caused by high temperatures, and also has a low shrinkage rate during molding (up to 150°C). In addition, it is characterized by low hygroscopicity, good electrical properties, color stability, good surface gloss and resistance to chemicals. Due to its good material properties, PBT is very widespread in the industry. For example, it is used in the electrical industry in the production of switches and connectors, in cooling fans, as a coil shaft in transformers and relays, and for the production of various types of caps, sensors and components housing components that must comply with regulations regarding the prevention of flame spread. In the automotive industry, it is used in the production of car bumpers, door handles, wipers and various electrical connectors, sockets,

switches, ignition system components, sensors as is the case with Yazaki. Type of PBT that will be analyzed in this thesis is Lanxess Pocan B3225, whose characteristics are known by [3] consisting of PBT as base material and 20% fiberglass (GF). Base material is PBT, Lanxess Pocan B1305, whose Young's modulus is $E = 2800$ MPa according to [4] , and Poisson's ratio $\nu = 0.3981$ according to [5]. Young's modulus and Poisson's ratio of glass fibers used is $E = 72400$ MPa [6], $\nu = 0.22$, the mean value was taken between 0.21 and 0.23 according to [7]. Stress-strain curves of Lanxes Pocan B3225 is shown in Figure 1.2.

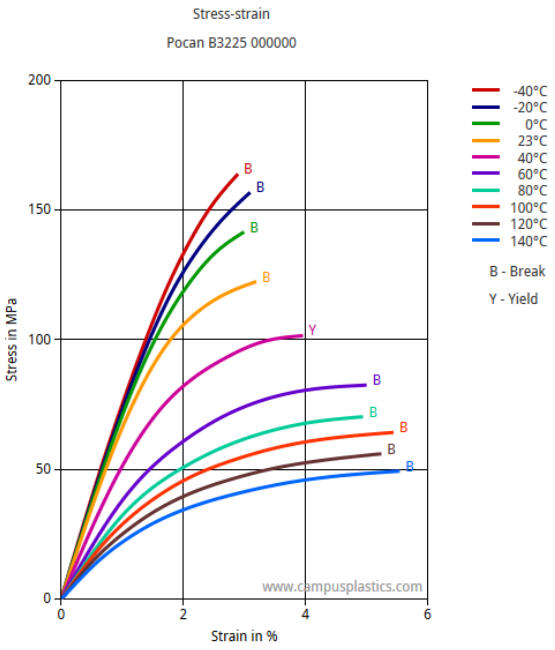

Figure 1.2 Stress-strain curves of Lanxess Pocan B3225 [3]

Glass fibers, which are added to the base material for the purpose of improving mechanical properties, have high chemical resistance, good insulation properties, are not flammable and are characterized by high strength. Contrary to the great advantages they bring, adding them increases the overall fragility of the material. In general, glass fibers can be divided according to their shape and material properties. In Lanxess Pocan B3225, GF that is used as reinforcement, is E-glass, which is made in form of thin lines with 14 μmm diameter, and average length of 150 μmm . Those type of GF is specific for high electrical resistance [6]. An example of such elongated glass fiber reinforced polymer is shown in Figure 1.3.

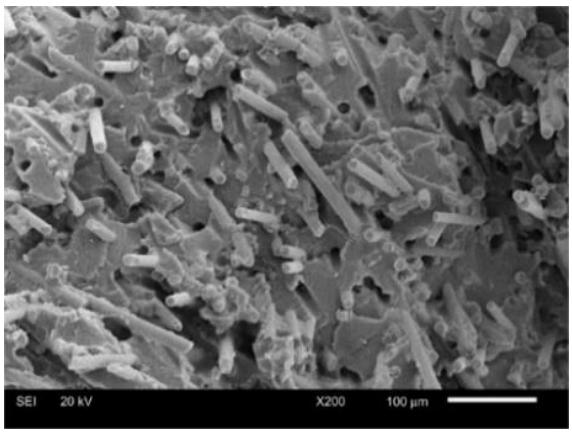

Figure 1.3 Microstructure of short glass fiber reinforced polymer

The injection molding process is used in the manufacture of such plastic molds. Among other things, such technology is used in the manufacture of items in the automotive industry, for plastic parts of household appliances and the production of simple plastic models. Injection molding is one of the most important cyclical plastic treatment processes. The process consists of the rapid injection of a plastomeric melt into a tempered mold cavity and its solidification into a workpiece. Since there is a possibility of process automation, this technology is suitable for large batch production of workpieces. The base material enters the melting cylinder by a hopper, which is heated with heaters. The screw catches it and it's activated by the hydro-motor. The moulded material is collected at top of the screw and when enough material is collected, the screw is moved by hydraulic cylinder forwards. After that, the injection of the melt through the nozzle into the mold begins. The melt is held under injection pressure and the material is cooled at the same time. After the injection process is complete, the mould is opened and the product is ejected [8]. A simplified injection moulding process is shown in Figure 1.4.

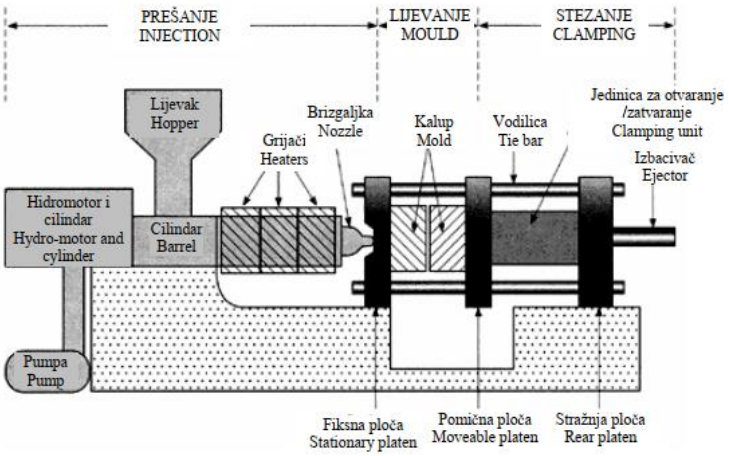

Figure 1.4 Simplified overview of machinery for injection moulding [8]

The injection molding process has great advantages, some of which are: high production productivity, possibility to produce objects of different volumes, relatively low production costs, possibility of process automation, production of objects of different surfaces, colors and finishing. Casting does not need to be post-treated.

While the benefits are great, there are some drawbacks to this technology. High cost of injection molding systems and accessories, casting quality is achieved only after a few cycles. There is also a large number of parameters that affect quality, such as temperature, pressure, dynamic viscosity [9]. Porosity can also occur, which is what is discussed in this thesis. Sinks and voids are caused by localized shrinkage of the resin at thick sections during the following steps:

- When excessively heated material expands to fill the mold cavity, it results in excess space between the plastic molecules.
- The skin of the material in the mold solidifies (freezes) first.
- As the remaining resin core cools and shrinks, it pulls the solidified skin with it away from the main mold wall.
- If the skin is sufficiently stiff, core shrinkage may not cause surface deformation but a void can form within the core of the resin as it shrinks.

Wall thickness strongly influences many key part characteristics, including mechanical performance and feel, cosmetic appearance, moldability, and economy. The optimum thickness is often a balance between opposing tendencies, such as strength versus weight reduction or durability versus cost [9]. (Figure 1.5)

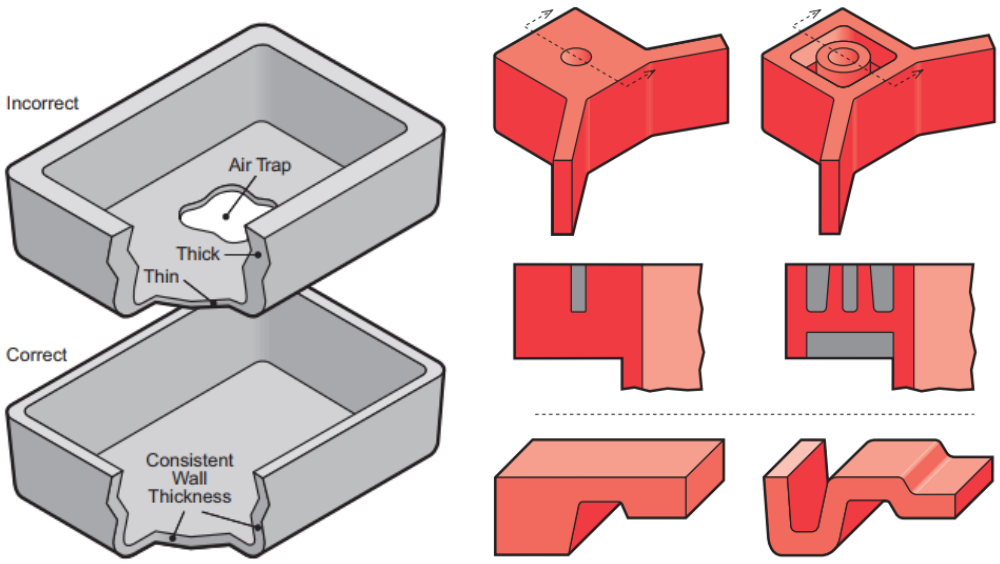

Figure 1.5 Examples of air traps caused by non-uniform wall thickness (right) and ways to design better to prevent such possibility (left) [9]

1.1 Anisotropy

While modeling material models with microscopic properties, it is fair to assume that material is no longer homogeneous and isotropic. In such case, anisotropy describes material that has different material properties in different directions. If material is fully anisotropic, each strain component depends linearly on all strain components. In that case, generalized Hooke's Law, for linear elastic material is shown in equation (1.1).

$$\begin{bmatrix} \sigma_1 = \sigma_{xx} \\ \sigma_2 = \sigma_{yy} \\ \sigma_3 = \sigma_{zz} \\ \sigma_4 = \sigma_{yz} \\ \sigma_5 = \sigma_{xz} \\ \sigma_6 = \sigma_{xy} \end{bmatrix} = \begin{bmatrix} C_{11} & C_{12} & C_{13} & C_{14} & C_{15} & C_{16} \\ C_{21} & C_{22} & C_{23} & C_{24} & C_{25} & C_{26} \\ C_{31} & C_{32} & C_{33} & C_{34} & C_{35} & C_{36} \\ C_{41} & C_{42} & C_{43} & C_{44} & C_{45} & C_{46} \\ C_{51} & C_{52} & C_{53} & C_{54} & C_{55} & C_{56} \\ C_{61} & C_{62} & C_{64} & C_{65} & C_{66} & C_{66} \end{bmatrix} \begin{bmatrix} \varepsilon_1 = \varepsilon_{xx} \\ \varepsilon_2 = \varepsilon_{yy} \\ \varepsilon_3 = \varepsilon_{zz} \\ \varepsilon_4 = \varepsilon_{yz} \\ \varepsilon_5 = \varepsilon_{xz} \\ \varepsilon_6 = \varepsilon_{xy} \end{bmatrix}. \tag{1.1}$$

This notation, with only one subscript for the stress and strain, numbered from 1…6, is helpful as it allows the equations of anisotropic elasticity to be written in matrix form. The 36 C_{ij} are material constants called stiffness matrix. These equations imply that a normal stress σ_{xx} will induce a material element to not only stretch in the direction and contract laterally, but to undergo shear strain too. Equation (1.1) can be inverted so that strains are given explicitly in terms of the stresses. The S_{ij} in Equation (1.2) are called compliances, and the matrix of compliances is called the compliance matrix. The bottom half of the compliance matrix has been omitted since it is symmetric.

$$\begin{bmatrix} \varepsilon_1 \\ \varepsilon_2 \\ \varepsilon_3 \\ \varepsilon_4 \\ \varepsilon_5 \\ \varepsilon_6 \end{bmatrix} = \begin{bmatrix} S_{11} & S_{12} & S_{13} & S_{14} & S_{15} & S_{16} \\ & S_{22} & S_{23} & S_{24} & S_{25} & S_{26} \\ & & S_{34} & S_{35} & S_{36} & S_{36} \\ & & & S_{45} & S_{46} & S_{46} \\ & & & & S_{56} & S_{56} \\ & & & & & S_{66} \end{bmatrix} \begin{bmatrix} \sigma_1 \\ \sigma_2 \\ \sigma_3 \\ \sigma_4 \\ \sigma_5 \\ \sigma_6 \end{bmatrix}. \tag{1.2}$$

In short notation, it can be written:

$$\sigma_i = C_{ij}\varepsilon_j \text{ and } \varepsilon_i = S_{ij}\sigma_j . \tag{1.3}$$

"An orthotropic material is one which has three orthogonal planes of microstructural symmetry. An example is shown in Figure 1.6a, which shows a glass-fibre composite material. The material consists of thousands of very slender, long, glass fibres bound together in bundles with oval cross-sections. These bundles are then surrounded by a plastic binder material. The continuum model of this composite material is shown in Figure 1.6b wherein the fine

microstructural details of the bundles and surrounding matrix are "smeared out" and averaged. Three mutually perpendicular planes of symmetry can be passed through each point in the continuum model. The x, y, z axes forming these planes are called the material directions."[10]

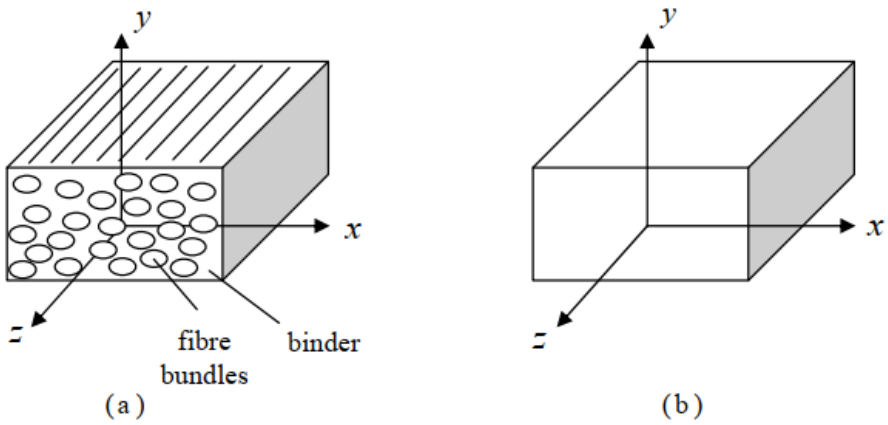

Figure 1.6 An orthotropic material; (a) microstructural detail, (b) continuum model [10]

The material symmetry inherent in the orthotropic material reduces the number of independent elastic constants. The stiffness matrix is reduced, and there are only nine independent elastic constants, as shown in equation (1.4).

$$\begin{bmatrix}\sigma_1\\ \sigma_2\\ \sigma_3\\ \sigma_4\\ \sigma_5\\ \sigma_6\end{bmatrix} = \begin{bmatrix} C_{11} & C_{12} & C_{13} & 0 & 0 & 0 \\ & C_{22} & C_{23} & 0 & 0 & 0 \\ & & C_{33} & 0 & 0 & 0 \\ & & & C_{44} & 0 & \\ & & & & C_{55} & \\ & & & & & C_{66} \end{bmatrix} \begin{bmatrix}\varepsilon_1\\ \varepsilon_2\\ \varepsilon_3\\ \varepsilon_4\\ \varepsilon_5\\ \varepsilon_6\end{bmatrix}. \tag{1.4}$$

These equations can be inverted to get, elastic constants E, ν and G in place of the S_{ij}:

$$\begin{bmatrix}\varepsilon_1\\ \varepsilon_2\\ \varepsilon_3\\ \varepsilon_4\\ \varepsilon_6\\ \varepsilon_6\end{bmatrix} = \begin{bmatrix} \frac{1}{E_1} & -\frac{\nu_{21}}{E_2} & -\frac{\nu_{31}}{E_3} & 0 & 0 & 0 \\ -\frac{\nu_{12}}{E_1} & \frac{1}{E_2} & -\frac{\nu_{32}}{E_3} & 0 & 0 & 0 \\ -\frac{\nu_{13}}{E_1} & -\frac{\nu_{23}}{E_2} & \frac{1}{E_3} & 0 & 0 & 0 \\ 0 & 0 & 0 & \frac{1}{2G_{23}} & 0 & 0 \\ 0 & 0 & 0 & 0 & \frac{1}{2G_{13}} & 0 \\ 0 & 0 & 0 & 0 & 0 & \frac{1}{2G_{12}} \end{bmatrix} \begin{bmatrix}\sigma_1\\ \sigma_2\\ \sigma_3\\ \sigma_4\\ \sigma_5\\ \sigma_6\end{bmatrix}. \tag{1.5}$$

An important feature of the orthotropic material is that there is no shear coupling with respect to the material axes. In other words, normal stresses result in normal strains only and shear stresses result in shear strains only.

A transversely isotropic material is one which has a single material direction and whose response in the plane orthogonal to this direction is isotropic. An example is shown in Figure 1.7, which again shows a glass-fibre composite material with aligned fibres, only now the cross-sectional shapes of the fibres are circular. The characteristic material direction is z and the material are isotropic in any plane parallel to the x - y plane. The material properties are the same in all direction's transverse to the fibre direction.

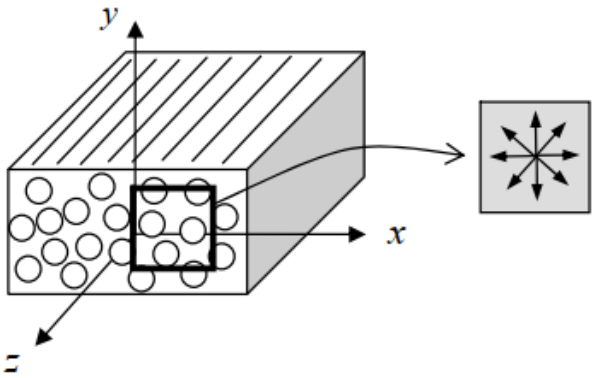

Figure 1.7 A transversely isotropic material [10]

Extra symmetry over that inherent in the orthotropic material reduces the number of independent elastic constants further. The stiffness matrix is thus reduced, and there are only five independent elastic constants:

$$\begin{bmatrix}\sigma_1\\ \sigma_2\\ \sigma_3\\ \sigma_4\\ \sigma_5\\ \sigma_6\end{bmatrix} = \begin{bmatrix} C_{11} & C_{12} & C_{13} & 0 & 0 & 0 \\ & C_{11} & C_{13} & 0 & 0 & 0 \\ & & C_{33} & 0 & 0 & 0 \\ & & & C_{44} & 0 & 0 \\ & & & & C_{44} & 0 \\ & & & & & C_{11}-C_{12} \end{bmatrix} \begin{bmatrix}\varepsilon_1\\ \varepsilon_2\\ \varepsilon_3\\ \varepsilon_4\\ \varepsilon_5\\ \varepsilon_6\end{bmatrix} \tag{1.6}$$

These equations can be inverted to get, introducing elastic constants E, ν and G in place of the Sij.

An isotropic material is one for which the material response is independent of orientation. The symmetry here further reduces the number of elastic constants to two, and the stiffness matrix reads

$$\begin{bmatrix}\sigma_1\\ \sigma_2\\ \sigma_3\\ \sigma_4\\ \sigma_5\\ \sigma_6\end{bmatrix}=\begin{bmatrix}C_{11} & C_{12} & C_{12} & 0 & 0 & 0\\ & C_{11} & C_{12} & 0 & 0 & 0\\ & & C_{11} & 0 & 0 & 0\\ & & & C_{11}-C_{12} & 0 & 0\\ & & & & C_{11}-C_{12} & 0\\ & & & & & C_{11}-C_{12}\end{bmatrix}\begin{bmatrix}\varepsilon_1\\ \varepsilon_2\\ \varepsilon_3\\ \varepsilon_4\\ \varepsilon_5\\ \varepsilon_6\end{bmatrix}. \tag{1.7}$$

Equations can now be inverted to get elastic constants E, ν and G,

$$\begin{bmatrix}\varepsilon_1\\ \varepsilon_2\\ \varepsilon_3\\ \varepsilon_4\\ \varepsilon_5\\ \varepsilon_6\end{bmatrix}=\begin{bmatrix}\frac{1}{E} & -\frac{\nu}{E} & -\frac{\nu}{E} & 0 & 0 & 0\\ -\frac{\nu}{E} & \frac{1}{E} & -\frac{\nu}{E} & 0 & 0 & 0\\ -\frac{\nu}{E} & -\frac{\nu}{E} & \frac{1}{E} & 0 & 0 & 0\\ 0 & 0 & 0 & \frac{1}{2G} & 0 & 0\\ 0 & 0 & 0 & 0 & \frac{1}{2G} & 0\\ 0 & 0 & 0 & 0 & 0 & \frac{1}{2G}\end{bmatrix}\begin{bmatrix}\sigma_1\\ \sigma_2\\ \sigma_3\\ \sigma_3\\ \sigma_5\\ \sigma_6\end{bmatrix}, \tag{1.8}$$

with,

$$\frac{1}{2G}=\frac{1+\nu}{E}. \tag{1.9}$$

2 Homogenization theory [11]

Heterogeneous materials are those materials consisting of a base material, a matrix, and additional phases, called inclusions. Inclusions can be varied and some of the most common ones are card fibers, micro-cavities or micro cracks. There are different types of such composite materials, some of which are thermoplastic polymers reinforced with short glass fibers (GFRP), rubber matrix composites (RMC), metal matrix composites (MMC) such as titanium reinforced with carbon or ceramic fibers, short steel fiber reinforced concrete, biomaterials. The goal is to perform micromechanical modeling to predict relationships between such microstructure and models at the macro level. One example of matrix with several stages of inclusions is shown in Figure 2.1.

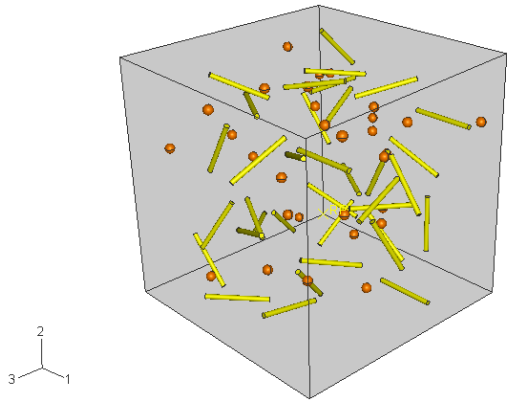

Figure 2.1 Matrix material reinforced with multiple phases of inclusions [11]

The objective of this theory is to predict the influence of the microstructure on the response of the body. Any heterogeneous solid body is consisted of matrix material phase and any number of inclusions phase that are subjected to given loads and boundary conditions (BCs). Computer solving of such mechanical problems, at the micro level, would be extremely demanding. Therefore, we distinguish two scales: the microscopic one (that of the heterogeneities) and the macroscopic one, where the solid can be seen as locally homogeneous. The link between the two scales is made via the concept of representative volume element (RVE). At macro scale, each material point is supposed to be the center of an RVE, which should be sufficiently large to represent the underlying heterogeneous microstructure, and small with respect to the size of the solid body. (Figure 2.2)

A two-scale approach which enables a transition between the two scales, both ways, is summarized in the following steps:

Micro – Macro transition:

1. Center of representative volume element (RVE) – Macro material point
2. At the micro level, RVE contains a finite number of constituents
3. For each of the constituents, a constitutive model is needed
4. Micro/macro transition is made with homogenization method to find macro constitutive response of RVE
5. Solving continuum mechanics problem at macro scale with macro constitutive equation

Macro – Micro transition:

1. At each time and at each macro material point, do a numerical zoom in order to see what happens at the micro level

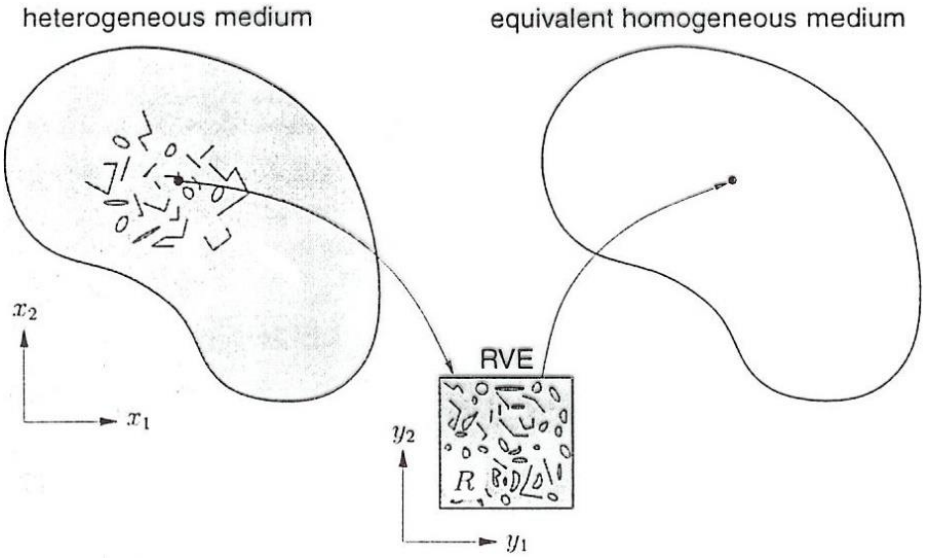

Figure 2.2 Micro – macro transition using representative volume element (RVE) [11]

Solving RVE problems at multi scale approach is major difficulty. Classical continuum mechanics analysis is carried out at macro level, which means that at each macro point **X**, we know the macro strain **E**(**X**) and need to compute the macro stress $\boldsymbol{\sigma}(\mathbf{X})$ or vice-versa. The average quantity over an RVE (domain ω, volume V) is defined by

$$\langle f(\mathbf{X},\mathbf{x})\rangle \equiv \frac{1}{V}\int_{\omega} f(\mathbf{X},\mathbf{x})dV\,, \tag{1.4}$$

where integration is performed with respect to micro coordinates, and f(**X, x**) is the micro field inside the RVE. In the following, dependence on macro coordinates *X* will be omitted for simplicity. We consider two classical types of BCs: (1) linear displacements, and (2) uniform traction. The former corresponds to a given macro strain (or more accurately an imposed macro displacement gradient) and the latter to a known macro stress.

At micro level, the boundary $\partial\omega$ of the RVE is subjected to imposed linear displacements:

$$u_i(\mathbf{x}) = G_{ij}x_j, \quad \mathbf{x} \in \partial\omega, \tag{1.5}$$

and the results is that the average strain equals the macro strain $\partial\omega$

$$\left\langle \varepsilon_{ij} \right\rangle = E_{ij}. \tag{1.6}$$

Macro stress σ is derived in the same way. At micro level, imposed traction on $\partial\omega$ is:

$$F_i(\mathbf{x}) = \sigma_{ij}n_j(\mathbf{x}), \quad \mathbf{x} \in \partial\omega, \tag{1.7}$$

where **n** is the outward unit normal to $\partial\omega$, and the results is that the average strain equals the macro stress:

$$\left\langle \sigma_{ij} \right\rangle = \sigma_{ij} \tag{1.8}$$

Representative volume elements (RVE) under classical boundary conditions has volume averages equal to macro strains and stresses.

From a continuum mechanics viewpoint, the problem of homogenization can be stated as follows: at the macro scale, in each macro material point, if we know the macro strain, we need to compute the macro stress, and vice-versa. From the above results, the following fundamental conclusion was reached:

Relating $\boldsymbol{E}$ and $\boldsymbol{\sigma}$ $\Leftrightarrow$ Relating $\langle\varepsilon\rangle$ and $\langle\sigma\rangle$.

In linear elasticity, the problem can be stated in a simpler form: find the macro stiffness such that $\langle\boldsymbol{\sigma}\rangle = \overline{\mathbf{C}} : \langle\varepsilon\rangle$. (Figure 2.3)

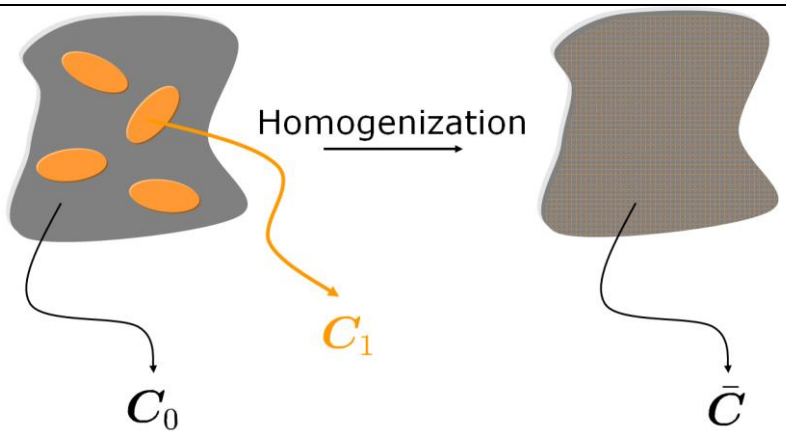

Figure 2.3 The idea of homogenization in linear elasticity [11]

The fundamental problem of homogenization in linear elasticity is to find an equivalent homogeneous material which has the same effective macro stiffness as the real heterogeneous composite, under the same boundary conditions. There are a few scale-transition methods which address this problem: asymptotic or mathematical homogenization theory, method of cells, sub cells and transformation field analysis, direct finite element analysis, and mean-field homogenization. The last two approaches will be used in this work.

2.1 Mean field homogenization (MFH)

The purpose of mean-field homogenization (MFH) is to compute approximate but accurate estimates of the volume averages of the stress and strain fields, both at the RVE level (macro stresses and strains) and in each phase. Mean-field homogenization does not solve the RVE problem in detail, and therefore does not compute the detailed micro stress and strain fields in each phase. There are many MFH models and each of them is based on some specific assumptions. Two simplest models are from Voigt and Reuss. Voigt model assumes that the strain field is uniform inside the RVE. Consequently, the macro stiffness is found to be the volume average of the micro stiffnesses. In the Reuss model, the stress field is assumed to be uniform in the RVE. Therefore, the macro compliance (the inverse of the stiffness) is found to be the volume average of the micro compliances. Voigt and Reuss models generalize the simple 1D models of bars in parallel, and in series, respectively. Both models are too simplistic. Indeed, assuming that strains or stresses are uniform within a composite is not realistic. Moreover, if each phase is isotropic, both models predict an isotropic composite, regardless of the shape and orientation of the inclusions, which is physically false. [11]

Method that will be used to determine the homogeneous properties of heterogeneous elastoplastic materials, is Mori-Tanaka (M-T). M-T belongs to one of the procedures for determining averaged values. M-T, as well as similar methods, are based on solving the problem of one equivalent inclusion which is embedded in base material whose dimensions are infinite. Base material undergoes nominal deformation, which is actually deformation tensor. Thus M-T assumes that equivalent inclusion is loaded with mean deformation value. [12], [13] Solution of Equivalent inclusion problem (EIP) is usually based on the Eshelby's solution. Solution says that inside infinite solid body of uniform stiffness $\mathbf{C}_o$ an ellipsoidal volume (*I*) is cut out, undergoes a stress-free eigenstrain ε^* and is then welded back into cavity it occupied. [14].

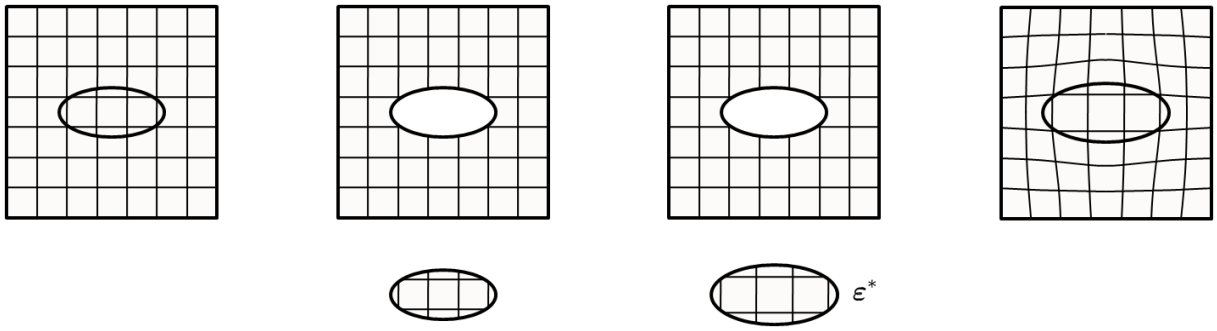

Figure 2.4 Representation of Eshelby's problem [11]

Eshelby found that the strain inside the ellipsoidal volume (*I*) is uniform and related to the eigenstrain as follows:

$$\varepsilon(\mathbf{x}) = \zeta\left(I, \mathbf{C}_0\right) : \varepsilon^*, \quad \forall \mathbf{x} \in (I) \tag{1.9}$$

where $\zeta(I, \mathbf{C}_0)$ is Eshelby's tensor. It depends on $\mathbf{C}_0$ and the shape (not the size) and orientation of (*I*). If $\mathbf{C}_0$ is isotropic and (*I*) is a spheroid (that is an ellipsoid of revolution), then the stiffness dependence is through Poisson's ratio only, and the shape dependence through the aspect ratio only. Eshelby's solution plays a fundamental role in MFH, as it enables to solve the single inclusion problem. [11].

The model that will be considered is simple two-phase composites made of a matrix material reinforced with any number of identical inclusions, having all the same material, shape and orientation. Subscript 0 will be used for matrix and 1 for the inclusion phase. The volume fractions in the two phases are such that $\nu_0 + \nu_1 = 1$. The volume averages of the strain field over the RVE, the matrix phase and the inclusion phase are related as follows:

$$\langle \varepsilon \rangle_{\omega} = \nu_0 \langle \varepsilon \rangle_{\omega_0} + \nu_1 \langle \varepsilon \rangle_{\omega_1} . \tag{1.10}$$

Any MFH model can be defined by so-called strain concentration tensors such that:

$$\langle \varepsilon \rangle_{\omega_1} = \mathbf{B}^{\varepsilon} : \langle \varepsilon \rangle_{\omega_0}, \quad \langle \varepsilon \rangle_{\omega_1} = \mathbf{A}^{\varepsilon} : \langle \varepsilon \rangle_{\omega} . \tag{1.11}$$

The volume average of strain over all inclusions is related to the volume average of strain over the matrix phase via the first tensor, and to the volume average of strain over the entire RVE (macro strain) with the second tensor. The two strain concentration tensors are not independent. The second one can be computed from the first one.

$$\mathbf{A}^{\varepsilon} = \mathbf{B}^{\varepsilon} : \left[\nu_1 \mathbf{B}^{\varepsilon} + (1-\nu_1)\mathbf{I} \right]^{-1} . \tag{1.12}$$

Equations (1.10),(1.11) and (1.12) are valid for any material model for either phase.

Next step is to introduce notation for two-phase linear elastic composites. For any homogenization model defined by a strain concentration tensor, the macro stiffness (sub. 0 for matrix and 1 for inclusions) is:

$$\overline{\mathbf{C}} = \left[\nu_1 \mathbf{C}_1 : \mathbf{B}^{\varepsilon} + (1-\nu_1)\mathbf{C}_0 \right] : \left[\nu_1 \mathbf{B}^{\varepsilon} + (1-\nu_1)\mathbf{I} \right]^{-1} . \tag{1.13}$$

Models of Voigt (uniform strain) and Reuss (uniform stress) correspond to the following choices respectively:

$$\mathbf{B}^{\varepsilon} = \mathbf{I} \quad \text{and} \quad \mathbf{B}^{\varepsilon} = \mathbf{C}_1^{-1} : \mathbf{C}_0 . \tag{1.14}$$

It is shown that the real composite's stiffness is bounded by the Voigt and Reuss estimates, which provide upper and lower bounds, respectively. In practice however, they are far-apart bounds, and therefore of little use. Tighter bounds do exist and are due to Hashin and Shtrikman.[15] Sophisticated MFH models or bounds closer than the Voigt and Reuss estimates all use a fundamental solution due to Eshelby.[14]

Using Eshelby's solution, single inclusion problem can now be solved. An infinite solid body is subjected to linear displacements on its boundary corresponding to a uniform remote strain **E**. The body is made of a matrix phase of uniform stiffness $\mathbf{C}_0$ in which is embedded a single ellipsoidal inclusion (*I*) of uniform stiffness $\mathbf{C}_1$. Based on Eshelby, strain inside the inclusion (*I*) is uniform and related to the remote strain as follows:

$$\varepsilon(\mathbf{x}) = \mathbf{H}^{\varepsilon}\left(I, \mathbf{C}_0, \mathbf{C}_1\right) : \mathbf{E}, \quad \forall \mathbf{x} \in (I) , \tag{1.15}$$

where $\mathbf{H}^{\varepsilon}$ is the single inclusion strain concentration tensor, defined as follows:

$$\mathbf{H}^{\varepsilon}\left(I,\mathbf{C}_0,\mathbf{C}_1\right)=\left\{\mathbf{I}+\zeta\left(I,\mathbf{C}_0\right):\mathbf{C}_0^{-1}:\left[\mathbf{C}_1-\mathbf{C}_0\right]\right\}^{-1}. \tag{1.16}$$

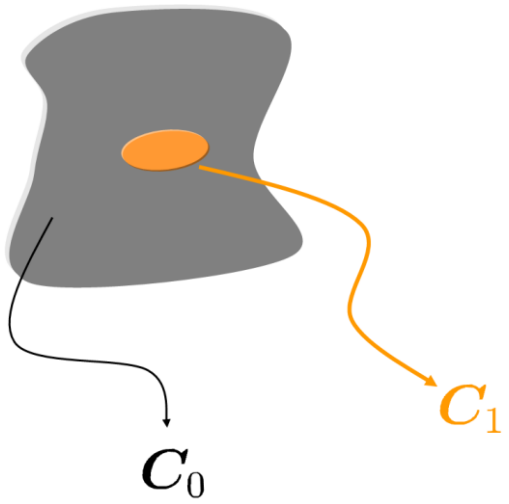

Figure 2.5 Single inclusion embedded in an infinite body [11]

Furthermore Hill's (polarization) tensor is defined as:

$$\mathbf{P}^{\varepsilon}\left(I,\mathbf{C}_0\right)=\zeta\left(I,\mathbf{C}_0\right):\mathbf{C}_0^{-1}. \tag{1.17}$$

Based on equations above, solution of single inclusion problem is cornerstone of any successful MFH model.

Finally, we can go back to the case of a composite RVE made of a matrix phase of uniform stiffness $\mathbf{C}_0$ reinforced with several inclusions of uniform stiffness $\mathbf{C}_1$, that are identical in terms of material, shape and orientation. Linear displacements corresponding to a remote strain E are imposed on the boundary. Unlike the single inclusion problem, this multi-inclusion problem does not have an analytical solution. Therefore, several MFH models exist based on different assumptions, but they all use the solution of single inclusion problem. Examples of such models are Self-consistent (S-C) model, Mori-Tanaka model, Double inclusion (D-I) model. [11]

2.1.1 Mori-Tanaka model

In 1973, Mori-Tanaka proposed a rational approach to correlate averaged stresses and strains of the constituent fiber with those of the matrix in a composite. Later in 1987, Benveniste [16] found that the Mori-Tanaka's approach can be reformulated by making use of the equivalent inclusion idea in terms of a more compacted tensor, that in a way only depends on an Eshelby's tensor. From this tensor, all of the effective elastic properties of composite can be

determined. Thus far, the Eshelby-Mori-Tanaka's method has become very popular for solving composite related problems.

As shown above strain concentration tensor relating the volume average of strain over all inclusions to the mean matrix strain is given by:

$$\mathbf{B}^{\varepsilon} = \mathbf{H}^{\varepsilon}\left(I, \mathbf{C}_0, \mathbf{C}_1\right), \tag{1.18}$$

which is exactly the strain concentration tensor of single inclusion problem. Each inclusion in the real RVE behaves as if it were isolated in the real matrix. The body is infinite and subjected to the average matrix strains in the real RVE as the far filed (remote) strain. This is illustrated in Figure 2.6. The M-T model is very successful in predicting the effective properties of two-phase composites. In theory, it is restricted to moderate volume fractions of inclusions (less than 25% say) but in practice it can give good predictions well beyond this range. [11].

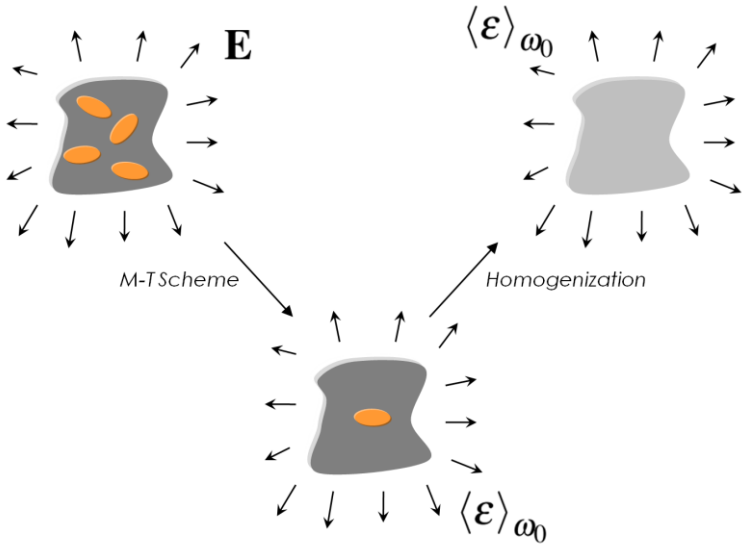

Figure 2.6 Illustration of the Mori-Tanaka (M-T) model [11]

3 Homogenization of PBT with 20% glass fibers (GF)

As already stated in the thesis, the material that will be analyzed is Lanxess Pocan B3225[3] which contains 20% glass fibers in form of long thin lines. First step, which will also be presented in this chapter, is, Mean-filed homogenization using Mori-Tanaka (M-T) method. The homogenization of such heterogeneous material will be carried out using the *Digimat* software package [17]. All necessary material characteristics are given in Table 1 below.

Table 1. Material characteristics of PBT and Glass fiber

	PBT (Lanxess PocanB3225[3])	Glass fiber (GF)
Volume fraction, V [%]	80	20
Young's modulus, E [MPa]	2800	72400
Poisson's ratio, v	0.3981	0.22
Diameter/length [mm]	-	$\phi 0.014 / 0.15$

Digimat can generate various types of inclusion geometries, that are shown in Figure 3.1. All of those shapes can be defined with aspect ratio L/D where L is length along the axis of revolution and D is diameter in the plane orthogonal to the axis of revolution, Changing the aspect ratio, any form of inclusion phase can be generated (with some limitations). Glass fiber inclusions are modeled with assumption of their cylindrical shape. Perfect cylindrical shape can't be chosen in MF (Mean-field homogenization) tool from *Digimat*, so inclusions will be modeled as elongated thin lines using *L/D* aspect ratio.

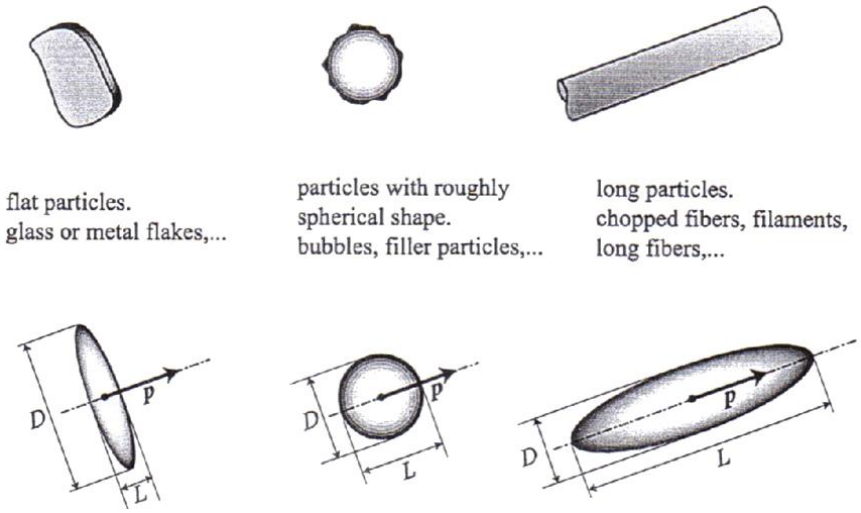

Figure 3.1 Various types of inclusions with a length smaller, equal or greater than diameter [11]

Fiber orientation is also a key parameter. There are three types of fiber orientation embedded in *Digimat* software. Uniaxial, 2D random, and 3D random. Uniaxial and 3D random are both specific for 2D and 3D RVE, 3D random is only present in 3D RVE. Uniaxial orientation means that all inclusions axis of revolutions are mutually parallel. 2D random orientation means that all inclusions are placed in multiple layers that are mutually parallel. Within each layer inclusions (fibers) are randomly placed. 3D random orientation means that all inclusions are randomly placed inside 3D space, that's why it can only be used in 3D RVE.

Digimat is supporting several strain loading variations. All analyzes performed in this thesis will be with uniaxial strain load. The component 11, of the macroscopic strain is driven manually. The other strain components are computed such that a macroscopic uniaxial stress state in the 1-direction is imposed. Load of 1.5% strain will be given to all models in this thesis.

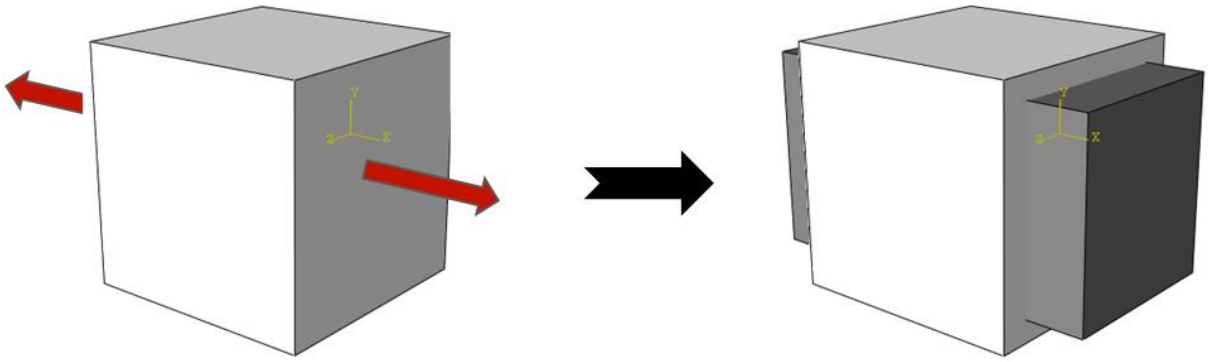

Figure 3.2 Illustration of the UNIAXIAL_1 loading

Linear elastic behavior of constituents and small deformations was assumed. It is known from the theory of elasticity that the relationship between stress tensors and deformations can be represented in a matrix form $\boldsymbol{\sigma} = \mathbf{C}\boldsymbol{\varepsilon}$, which is shown in a form below:

$$\begin{pmatrix} \sigma_{11} \\ \sigma_{22} \\ \sigma_{33} \\ \sigma_{33} \\ \sigma_{12} \\ \sigma_{13} \\ \sigma_{23} \end{pmatrix} = \frac{E}{(1+\nu)(1-2\nu)} \begin{pmatrix} 1-\nu & \nu & \nu & 0 & 0 & 0 \\ \nu & 1-\nu & \nu & 0 & 0 & 0 \\ \nu & \nu & 1-\nu & 0 & 0 & 0 \\ 0 & 0 & 0 & \frac{1-2\nu}{2} & 0 & 0 \\ 0 & 0 & 0 & 0 & \frac{1-2\nu}{2} & 0 \\ 0 & 0 & 0 & 0 & 0 & \frac{1-2\nu}{2} \\ & & & & 2 & \end{pmatrix}. \tag{3.1}$$

By incorporating the material properties of fiberglass reinforced PBT into the elastic matrix according to (3.1), the elasticity matrix of PBT with 20% fiber glass follows:

$$\mathbf{C} = \begin{pmatrix} 11714 & 6478 & 6478 & 0 & 0 & 0 \\ 6478 & 11714 & 6478 & 0 & 0 & 0 \\ 6478 & 6478 & 11714 & 0 & 0 & 0 \\ 0 & 0 & 0 & 2617 & 0 & 0 \\ 0 & 0 & 0 & 0 & 2617 & 0 \\ 0 & 0 & 0 & 0 & 0 & 2617 \end{pmatrix}. \tag{3.2}$$

Using Mori-Tanaka homogenization method embedded in *Digimat*, elastic matrix, for all three types of inclusion orientation is given below:

$$|\mathbf{C}^{\text{Uniaxial}} = \begin{pmatrix} 13940 & 4650 & 4650 & 0 & 0 & 0 \\ 4650 & 7594.1 & 4788.4 & 0 & 0 & 0 \\ 4650 & 4788.4 & 7594.1 & 0 & 0 & 0 \\ 0 & 0 & 0 & 1474.3 & 0 & 0 \\ 0 & 0 & 0 & 0 & 14029 & 0 \\ 0 & 0 & 0 & 0 & 0 & 1474.3 \end{pmatrix}, \tag{3.3}$$

$$\mathbf{C}^{\text{2D random}} = \begin{pmatrix} 9974.8 & 5442.1 & 4719.2 & 0 & 0 & 0 \\ 5442.1 & 9974.8 & 4719.2 & 0 & 0 & 0 \\ 4719.2 & 4719.2 & 7594.1 & 0 & 0 & 0 \\ 0 & 0 & 0 & 2266.4 & 0 & 0 \\ 0 & 0 & 0 & 0 & 1438.6 & 0 \\ 0 & 0 & 0 & 0 & 0 & 1438.6 \end{pmatrix}, \tag{3.4}$$

$$|\mathbf{C}^{\text{3D random}} = \begin{pmatrix} 8864.4 & 5118.6 & 5118.6 & 0 & 0 & 0 \\ 5118.6 & 8864.4 & 5118.6 & 0 & 0 & 0 \\ 5118.6 & 5118.6 & 8864.4 & 0 & 0 & 0 \\ 0 & 0 & 0 & 1872.9 & 0 & 0 \\ 0 & 0 & 0 & 0 & 1872.9 & 0 \\ 0 & 0 & 0 & 0 & 0 & 1872.9 \end{pmatrix}. \tag{3.5}$$

Comparing the matrix from (3.3),(3.4) and (3.5) with (3.2), it's possible to notice that uniaxial fiber orientation is giving stiffer mechanical properties, unlike 2D and 3D random orientation which are giving lower values in stiffness matrix.

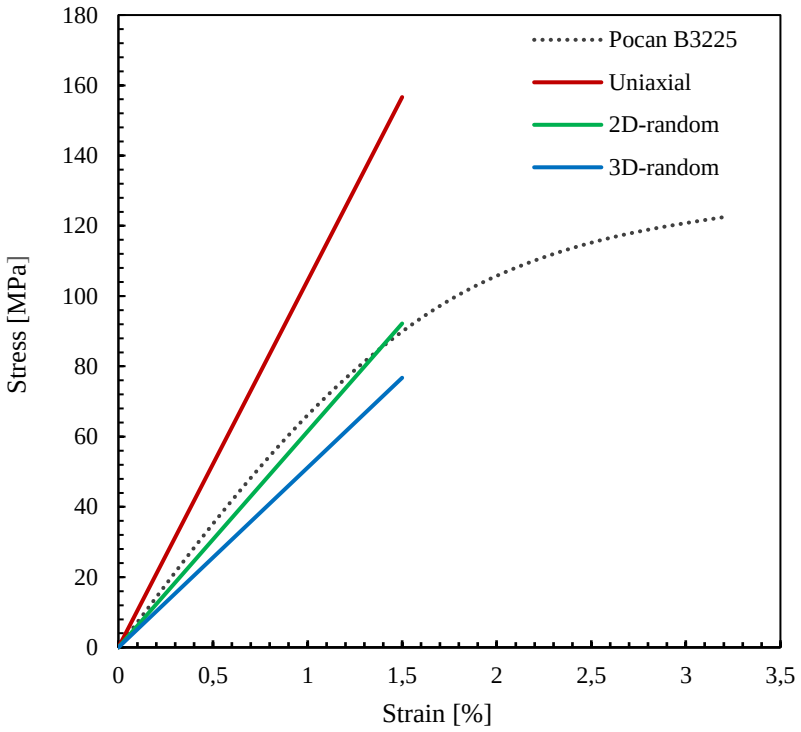

Figure 3.3 Comparison of Mean-field homogenization using *Digimat* with experimental results of Pocan B3225

Using *Digimat*'s mean field homogenization method, stress-strain values for all three types of fiber orientation were obtained and shown in Figure 3.3. and compared with Pocan's B3225 stress-strain values. As expected, biggest stiffness was given by model with uniaxial fiber orientation, because fibers were oriented in the same axis as given load. 2D random orientation model had the closest match with experimental results of Pocan B3225.

4 Finite element analysis of PBT with 20% glass fibers (GF)

After analysis using the MFH method and the results presented, the next step is to repeat the similar procedure using the finite element method. The biggest difference is that actual geometry will be generated using *Digimat*-FE tool, which is essentially a finite element-based homogenization module of *Digimat*. The actual macro-level geometry will be replaced by a representative volume element (RVE) that will represent it. Several RVEs of equal dimensions will be generated for each case and the results will be compared to the actual results of the Lanxess Pocan B3225. The goal will be to find the RVE after which further increase of its geometry does not change the result. The *Digimat* FE tool will be used to add material properties to phases. An abbreviated analysis procedure for one of the RVEs is:

1. Defining material characteristics according to Table 1
2. Adding material and volume fraction to each of the phases and defining the geometric characteristics of the inclusions also according to Table 1
3. Defining the size of the RVE and generating geometry for each of the inclusion orientation case
4. Defining mesh settings
5. Defining boundary conditions
6. Defining load - 1.5% axial strain
7. Exporting .py script using *Digimat*-FE tool
8. Importing .py script in Abaqus by which the .cae model is generated
9. Performing linear-elastic analysis to obtain averaged material stress and strain values

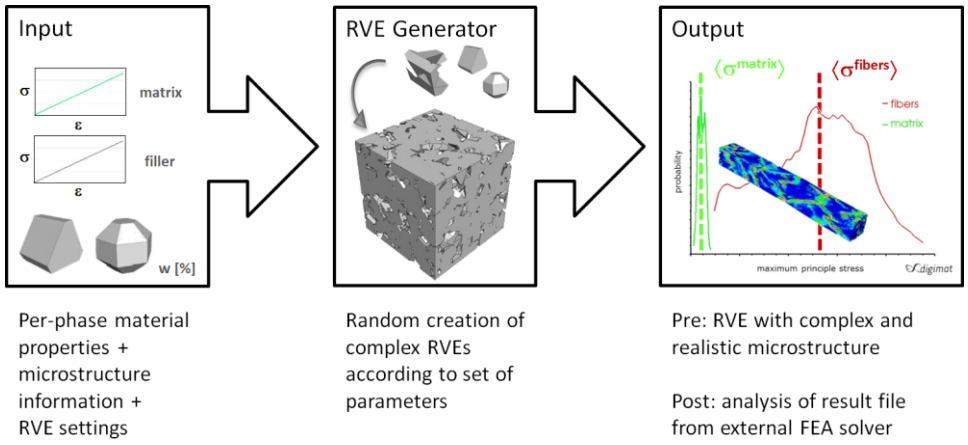

Figure 4.1 ***Digimat*-FE general workflow** [11]

On Figure 4.1, general workflow of *Digimat* FE tool is shown in short steps. As already stated above, all necessary inputs are given in Table 1. Unlike the *Digimat* MF tool, in the FE tool it is possible to define the correct geometry independently of the L / D aspect ratio Given the elongated shape of the glass fibers, cylindrical and sphero-cylinder shape of fibers is chosen into consideration as Figure 4.2 shows. After several analyzes with both types of fibers, it was decided that the analysis would be performed with cylindrical inclusions, because fibers with spherical cylindrical ends have greater problems with the meshing of such rounded tips.

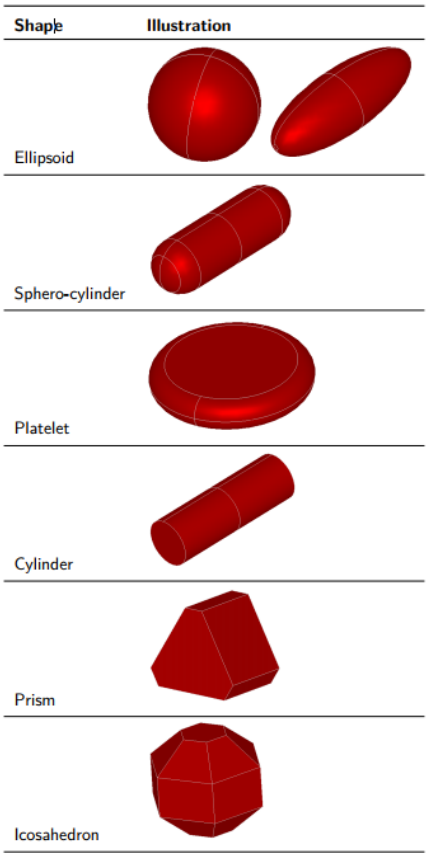

Figure 4.2 Available predefined inclusions shape in *Digimat* [11]

Analyzed geometry will be 2D and 3D with fiber orientation specified in Chapter 3. The RVE will be cube-shaped with 4 different sizes and its length will be 0.16 mm, 0.2 mm, 0.25 mm and 0.3 mm in all three axes. The main goals when generating an RVE will be to meet the default glass fiber volume fraction of 20%. The parameters that will change as needed are minimum relative distance between inclusions and minimum relative volume. Minimum relative distance between inclusions, as shown on Figure 4.3, is defining what will be minimum distance between placed inclusions inside RVE. The effective distance is computed based on the size of current inclusion. This can be useful to avoid geometries difficult to mesh. [11]

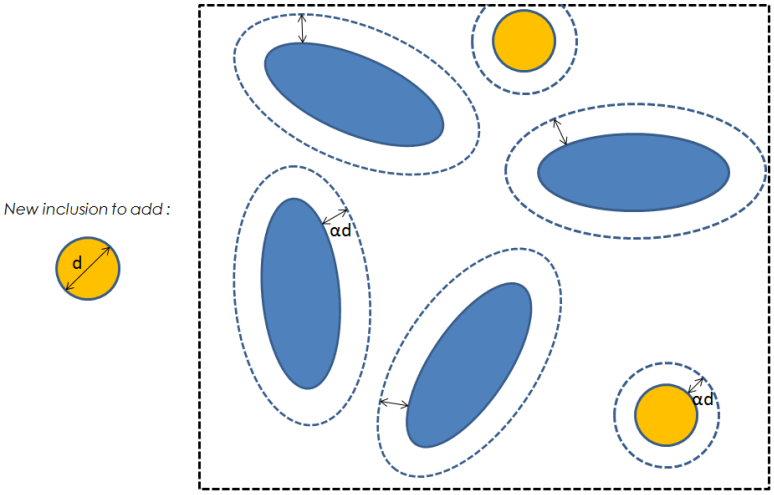

Figure 4.3 Concept of minimum relative distance between inclusions [11]

Minimum relative volume is also value that can be used to avoid geometries difficult to mesh. When inclusions are intersecting with the faces of the RVE or interpenetrating with other inclusions, some parts of the inclusion are removed. If the volume of the remaining part is less than the specified value, then this inclusion is discarded. The specified value is relative to the initial volume of the current inclusion. If a value of 1 is specified, no intersection between the inclusions and the faces of the RVE will be allowed, i.e., all the inclusions will lie fully inside the RVE. This concept is shown on Figure 4.4.

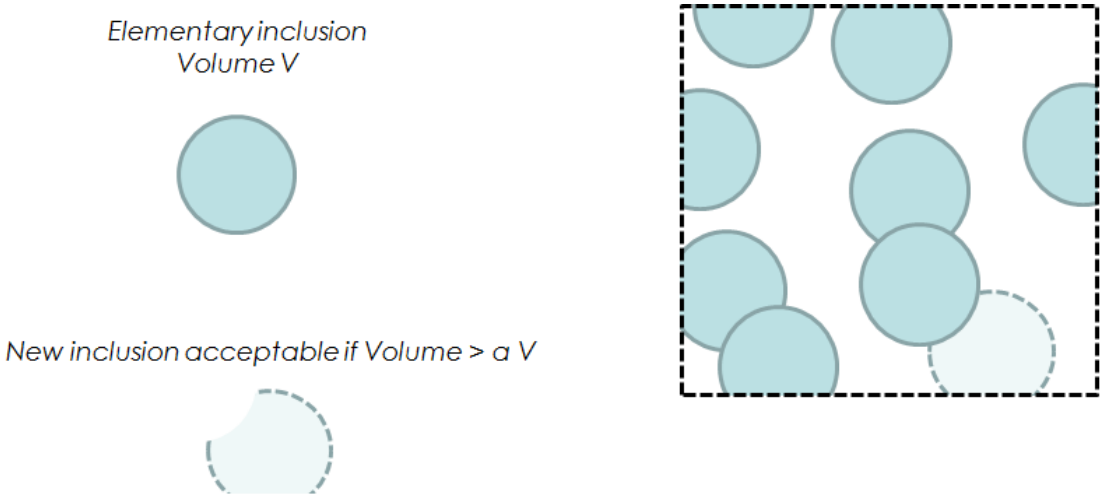

Figure 4.4 Illustration of concept of minimum relative volume [11]

Geometry and boundary conditions were modeled as periodic, because that kind of analysis can lead to best predictions when compared to the Dirichlet and Mixed boundary condition type. "This model ensures faster convergence rate as the size of the volume element increases, but to the expense of increased CPU time and memory requirements to solve finite element problem."

[11] Periodic geometry is mainly used so periodic boundary conditions can be implemented. Any inclusion intersecting one of the RVE faces will have its complement placed periodically in the RVE, such that opposite faces look identical. Figure 4.5

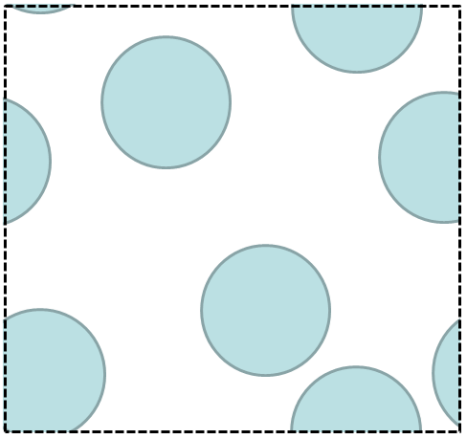

Figure 4.5 2D example of periodic geometry [11]

In combination with periodic geometry, periodic boundary conditions can also be used that will ensure that the flux of the filed variable (in this case displacement) is periodic with respect to the faces of the volume element. "This is enforced through a large set of equations relating the degrees of freedom of the nodes lying on one face with those of the corresponding nodes lying on the opposite face, on a 2-by-2 basis. Node duplication is used to prevent issues coming from non-periodic meshes. This all can lead to decrease of performance due to the potentially large set of constraint equations that has to be imposed. Figure 4.6 illustrates the definition of periodic boundary conditions in the case of a mechanical loading with macroscopic uniaxial peak strain ε_{11}." [11].

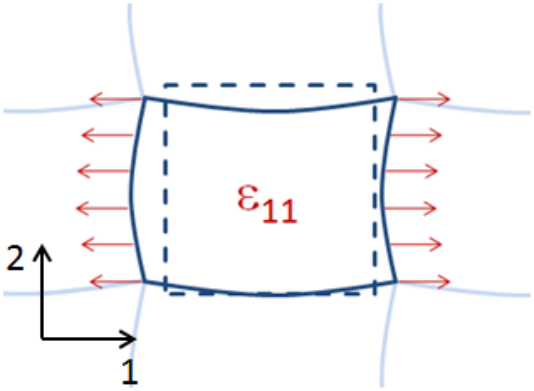

Figure 4.6 Periodic boundary condition type [11]

4.1 Finite element method (FEM)

The finite element method (FEM) is a method based on physical discretization of continuum. Classical methods are based on solving differential equations, of which analytical solution can only be obtained for simpler models. In general, it's very difficult to obtain solution that satisfies differential equations. Therefore, approximate numerical methods are used, with which differential equations are replaced by algebraic equations. Chosen continuum with infinite degrees of freedom is replaced with discrete model that has interconnected elements with limited numbers degrees of freedom. More specifically, observed continuum was described with finite element mesh. Such finite elements are interconnected at points on contour, that are called nodes. The state of each element, such as displacement, deformation, stress, temperature, etc., is described using interpolation functions. These functions must satisfy the appropriate conditions to bring the discretized model as close as possible to the behavior of continuum. With the correct formulation of finite elements, the approximation to the exact solution grows with increasing number of elements. The finite element method allows us to find a numerical solution to a specific problem. The solution is not an equation but a pure numerical value. The solution obtained is usually approximate, unless the problem is so simple that there is a derived formula for it. Complex constructions require discretization with many elements and the system must be solved using algebraic equations with many unknowns, which is very difficult to achieve without using a computer. Therefore, it is necessary to use specific computer programs in order solve problem using finite element method. For that purpose, many CAE (Computer Aided Engineering) software packages were made and some of them are *ABAQUS, ANSYS or MSC Nastran/Patran*. Derivation of finite element equations can be quite complex, but the use of these finite elements within said software packages is quite simple. Those programs are designed to, in most cases, provide some solution that may not be physically accurate. Depending on the shape and unknown parameters in nodes, different types of finite elements was derived. Basic finite elements most commonly applied in deformable mechanics bodies are shown in Figure 4.7. [18][19][20].

As shown in Figure 4.7, there are many types of finite elements, but only 2 types of elements will be used in this thesis, depending on whether a 2D or 3D problem is analyzed. CPE8R for 2D problems and C3D10M for 3D problems.

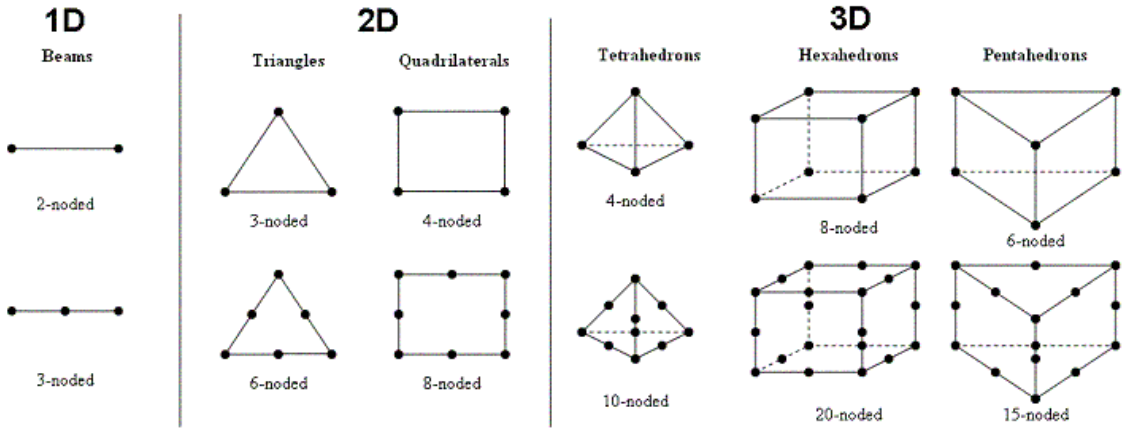

Figure 4.7 List of basic finite elements [21]

4.2 Formulation of CPE8R and C3D10M elements

CPE8R is 8-node biquadratic plane strain continuum elements with reduced integration. CPE8 element is shown in Figure 4.8.

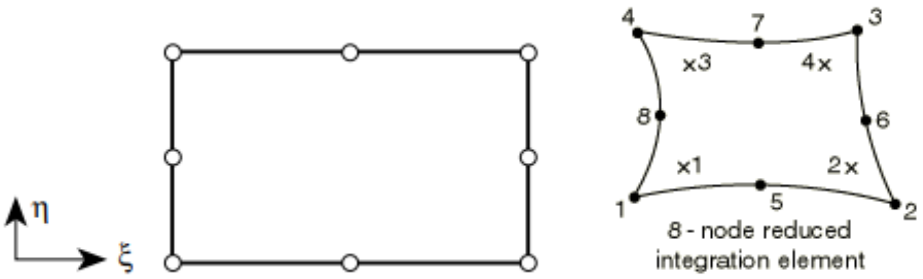

Figure 4.8 8-node biquadratic plane strain element (left) and with reduced integration (right) [22]

Corner nodes:

$$N_a = \frac{1}{4}(1+\xi_a\xi)(1+\eta_a\eta)(\xi_a\xi+\eta_a\eta-1). \tag{4.1}$$

Mid – side nodes:

$$\begin{aligned} \xi_a = 0 \quad & N_a = \frac{1}{2}(1-\xi^2)(1+\eta_a\eta) \\ \eta_a = 0 \quad & N_a = \frac{1}{2}(1+\xi_a\xi)(1-\eta^2) \end{aligned}, \tag{4.2}$$

where subscript *a* is node designation.

C3D10 is 10 node quadratic tetrahedral element (Figure 4.9) and it is used in general purpose analysis. Biggest disadvantage is that they do not yield desirable results when used with finite

sliding, node to surface formulation and direct enforcement method. Better performance in such cases can be achieved with C3D10M, which is also used in this thesis. C3D10M are "modified" formulation elements using bilinear interpolation. [23]

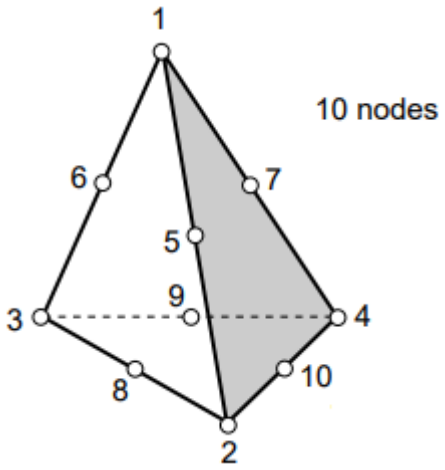

Figure 4.9 10-node quadratic tetrahedron C3D10 [22]

Displacement components in Cartesian's coordinate system is given in equations (4.3):

$$\begin{aligned} u &= a_1 + a_2x + a_3y + a_4z + a_3x^2 + a_6y^2 + a_7z^2 + a_8xy + a_9yz + a_{10}xz \\ v &= a_{11} + a_{12}x + a_{13}y + a_{14}z + a_{15}x^2 + a_{16}y^2 + a_{17}z^2 + a_{18}xy + a_{19}yz + a_{20}xz \\ w &= a_{21} + a_{22}x + a_{33}y + a_{24}z + a_{25}x^2 + a_{24}y^2 + a_{27}z^2 + a_{28}xy + a_{24}yz + a_{10}xz \end{aligned} \quad . \tag{4.3}$$

Shape functions are derived in same way as for basic tetrahedral element. The kinematic operator for calculating matrix B contains only the first two derivatives, which means that order of the functions describing the deformation distribution is by one row lower than the order of the displacement distribution function. C3D10 element can describe a linear field of deformations, which is same order as field of stress. [20].

Shape for corner nodes are defined as:

$$N_a = \left(2L_a - 1\right)L_a \quad a = 1,2,3,4\,, \tag{4.4}$$

and for mid-edge nodes:

$$N_5 = 4L_1L_2\,. \tag{4.5}$$

L_1 is defined as:

$$L_1 = \frac{\text{volume } P234}{\text{volume } 1234}\,, \tag{4.6}$$

which also follows for L_2, L_3 and L_4 based in Figure 4.10.

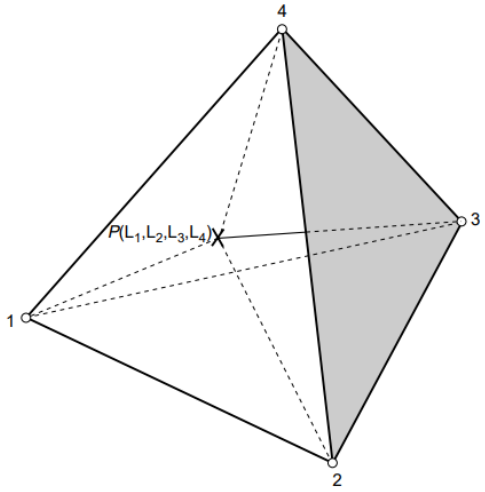

Figure 4.10 Tetrahedron volume coordinates [22]

4.3 Finite element analysis of PBT with 20% glass fibers

In this section, finite element analysis on a representative volume element (RVE) will be conducted to demonstrate that its averaged properties realistically describe the mechanical behavior of macro components. 2D RVE analysis will be performed first and then 3D. All results will be compared to the $\sigma - \varepsilon$ diagram of Lanxess Pocan B3225. The average fiber length is 0.15 mm so that all fibers will be dimensioned with that value. First size of the RVE will be 0.16 mm and is taken to be slightly larger than the length of the fiber to allow sufficient space between the start and end points of the fiber since periodic geometry and boundary conditions will be used. Three types of fiber glass orientation will be analyzed:

1. Uniaxial – directions of all fibers are equal (used in 2D and 3D RVE)
2. 2D random - inclusions are placed in multiple layers that are mutually parallel and within each layer inclusions (fibers) are randomly placed (used in 2D and 3D RVE)
3. 3D random – inclusions are placed random in 3D space (used only in 3D RVE)

4.4 Finite element analysis of 2D RVE

As mentioned before, the generation of geometry with loads and boundary conditions will be carried out in the *Digimat*-FE tool. 4 different size geometries will be generated 0.16 mm, 0.2 mm, 0.25 mm, 0.3 mm. All the necessary material and geometric characteristics are given in Table 1.

4.4.1 2D RVE, Uniaxial fibers orientation analysis

In this section will be shown all results from 2D RVE with uniaxial fiber orientation.

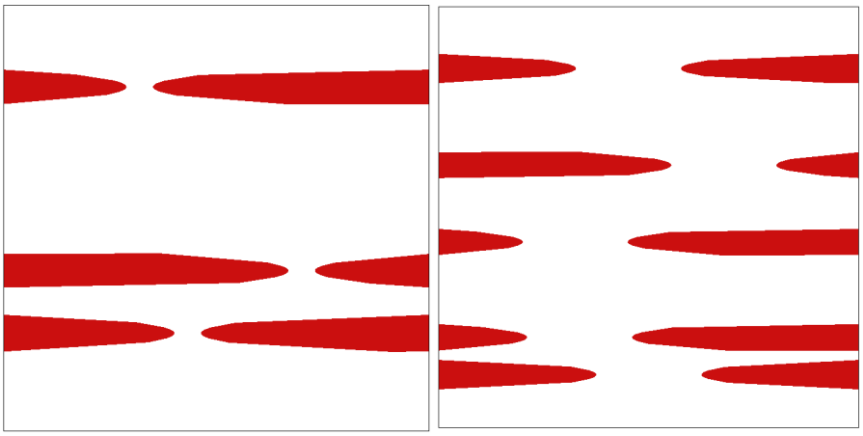

Figure 4.11 2D RVE, Uniaxial orientation: 0.16 mm (left) and 0.2 mm (right)

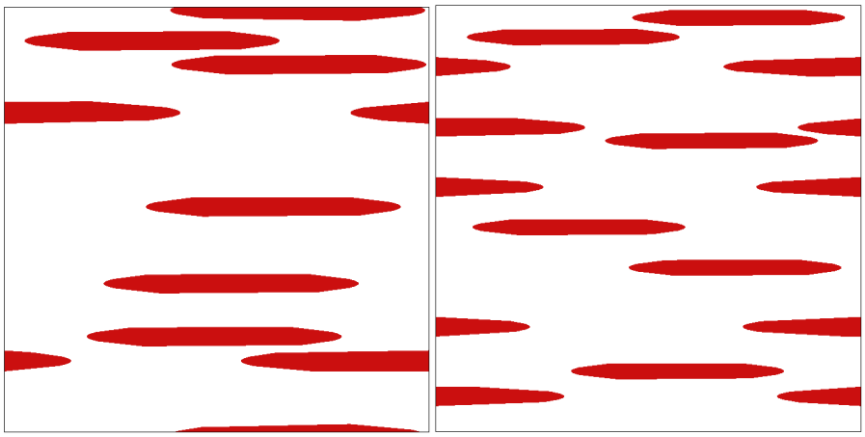

Figure 4.12 2D RVE geometry, Uniaxial orientation: 0.25 mm (left) and 0.3 mm (right)

In Figure 4.11 and Figure 4.12, the 2D RVE geometries are randomly generated with *Digimat*-FE tool.

All four RVE were modeled with the periodic boundary conditions and load. Given load is 1.5% strain in axis parallel to fibers. Next step is to generate Python script, and import in software package Abaqus. [24]. The values of number of inclusions in each RVE and volume fraction achieved in each case are given in Table 2.

Table 2 Number of inclusions and achieved volume fraction of 2D RVE, Uniaxial fiber orientation

	1.RVE 0.16 mm	2.RVE 0.2 mm	3.RVE 0.25 mm	4.RVE 0.3 mm
Number of inclusions	3	5	8	11
Effective volume fraction [%]	0.193347	0.206624	0.211687	0.201967

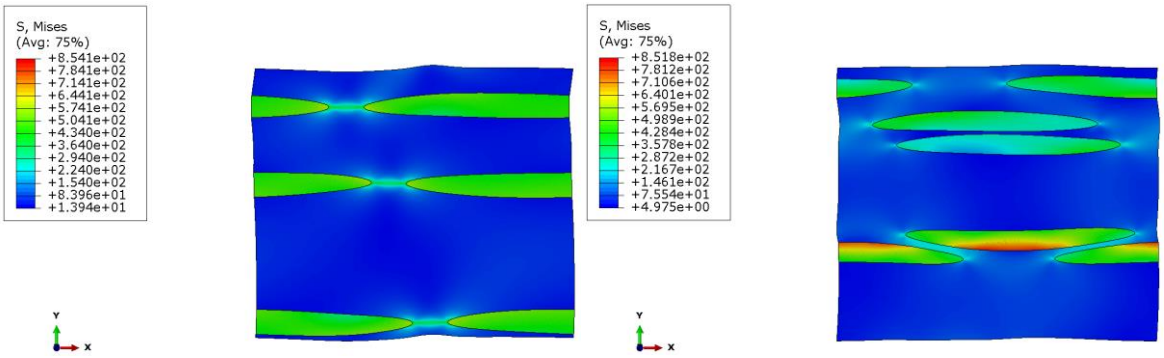

Figure 4.13 2D RVE results, Uniaxial orientation: 0.16 mm (left) and 0.2 mm (right)

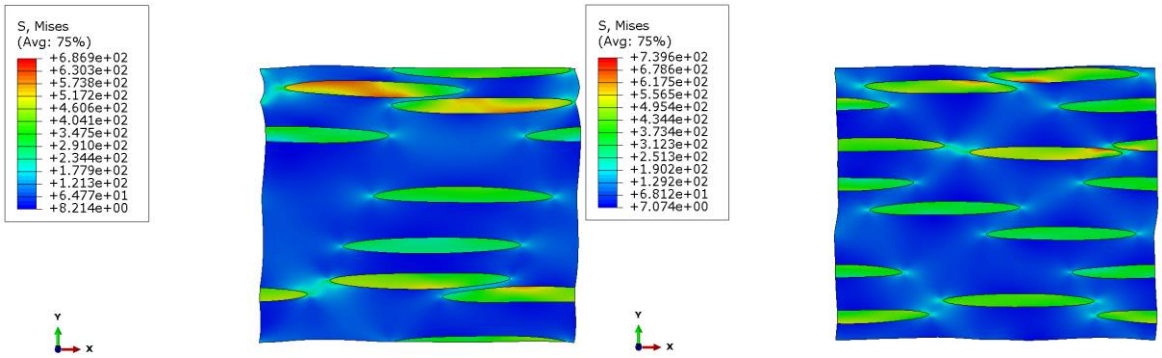

Figure 4.14 2D RVE results, Uniaxial orientation: 0.25 mm (left) and 0.3 mm (right)

Figure 4.13 and Figure 4.14 shows results of all four analysis that were conducted in software package Abaqus. Table 3 shows number of finite elements generated per each RVE generated.

Table 3 Number of finite elements per each RVE generated, 2D RVE, Uniaxail

	1.RVE 0.16 mm	2.RVE 0.2 mm	3.RVE 0.25 mm	4.RVE 0.3 mm
Number of CPE8R	49 213	49 089	50 000	51 738

In order to get volumetric mean values for stress and strain, *Digimat* FE tool was used. Results from Abaqus was loaded into *Digimat* FE and post-process was made. Volumetric mean results of stress strain values were compared with Pocan B3225, and shown in Figure 4.15.

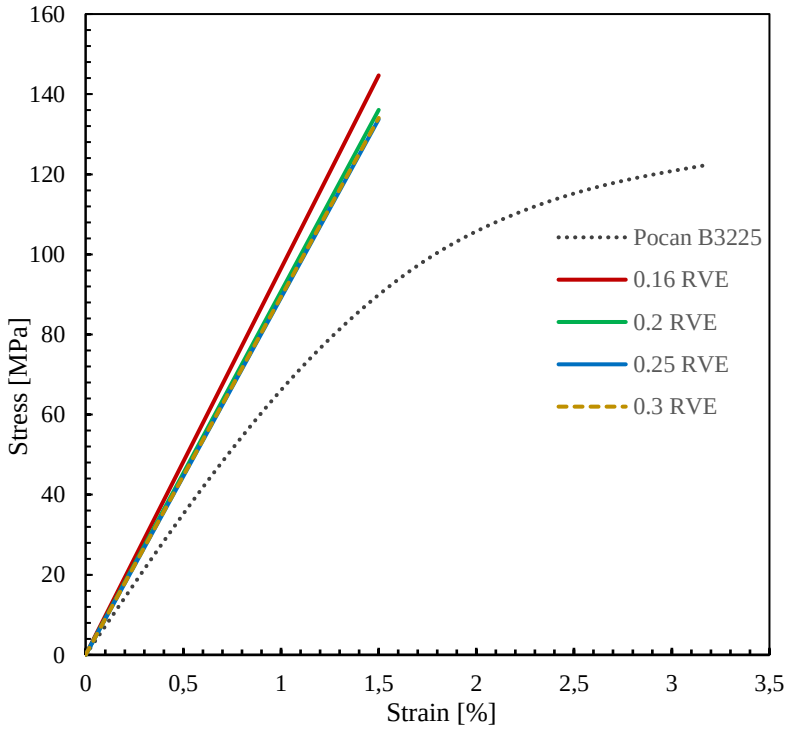

Figure 4.15 Stess-strain results for 2D RVE, Uniaxial fiber orientation

As shown in Figure 4.15, stiffness of each modeled RVE is noticeably higher than Pocan B3225, because fibers were oriented in same way as given load. Since fibers have the highest stiffness in the direction of their elongation, this orientation mode gives a stiffness greater than the material. Mean filed homogenization also gave similar results for uniaxial fiber orientation (Figure 3.3)

4.4.2 2D RVE, random fibers orientation analysis

Same procedure will be made for 2D RVE, but with different fiber orientation. Fibers will be placed randomly inside given RVE. Periodic boundary conditions and load were also given. Figure 4.16 and Figure 4.17 shows all four RVE geometries generated and in Table 4 and Table 5 were given information about number of inclusions per RVE, achieved volume fraction and number of finite elements per each mesh.

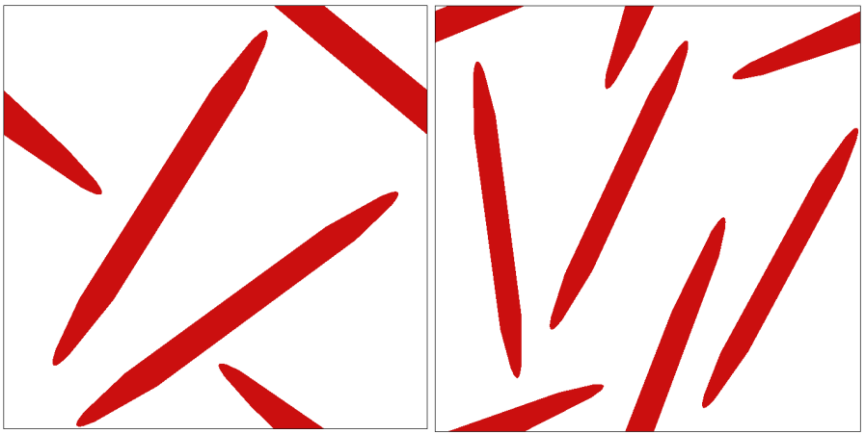

Figure 4.16 2D RVE, random fiber orientation: 0.16 mm (left) and 0.2 mm (right)

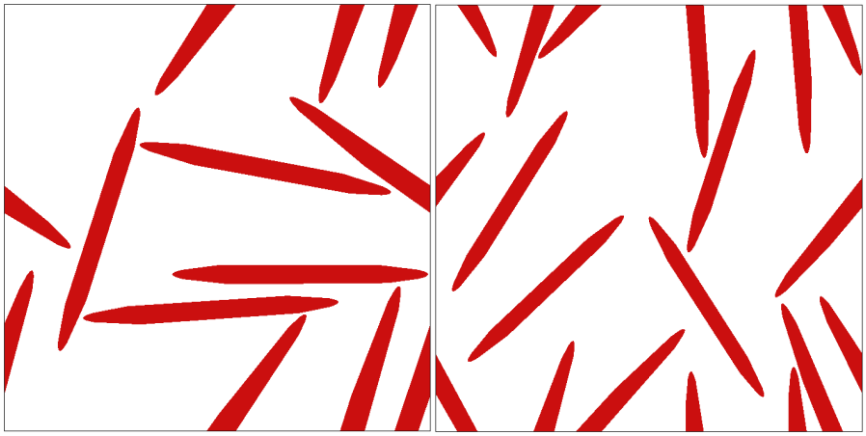

Figure 4.17 2D RVE, random fiber orientation: 0.25 mm (left) and 0.3 mm (right)

Table 4 Inclusion number and achieved volume fraction of 2D RVE, 2D random fiber orientation

	1.RVE 0.16 mm	2.RVE 0.2 mm	3.RVE 0.25 mm	4.RVE 0.3 mm
Number of inclusions	3	5	8	11
Effective volume fraction [%]	0.193347	0.206624	0.211479	0.201794

Table 5 Number of finite elements per each RVE generated, 2D RVE, 2D random fiber orientation

	1.RVE 0.16 mm	2.RVE 0.2 mm	3.RVE 0.25 mm	4.RVE 0.3 mm
Number of CPE8R	49 087	49 308	50 269	51 473

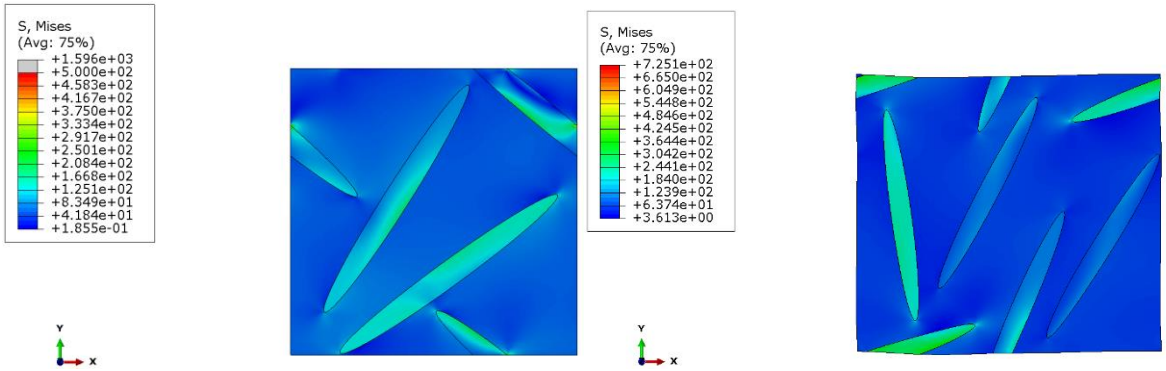

Figure 4.18 2D RVE results, random fiber orientation: 0.16 mm (left) and 0.2 mm (right)

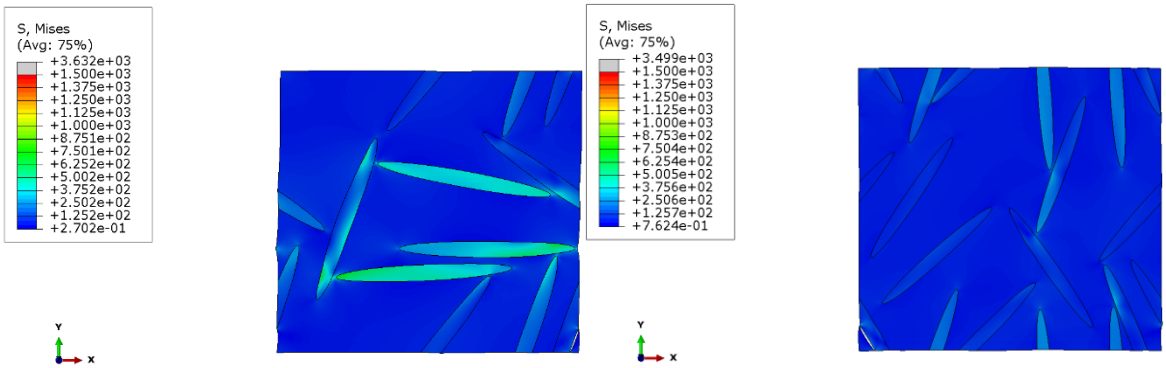

Figure 4.19 2D RVE results, random fiber orientation: 0.25 mm (left) and 0.3 mm (right)

Figure 4.18 and 19 shows results after conducted analysis. Mean values for stress and strain are shown in Figure 4.20. Random fiber orientation is giving closer approximation of stress-strain curve in linear elastic domain.

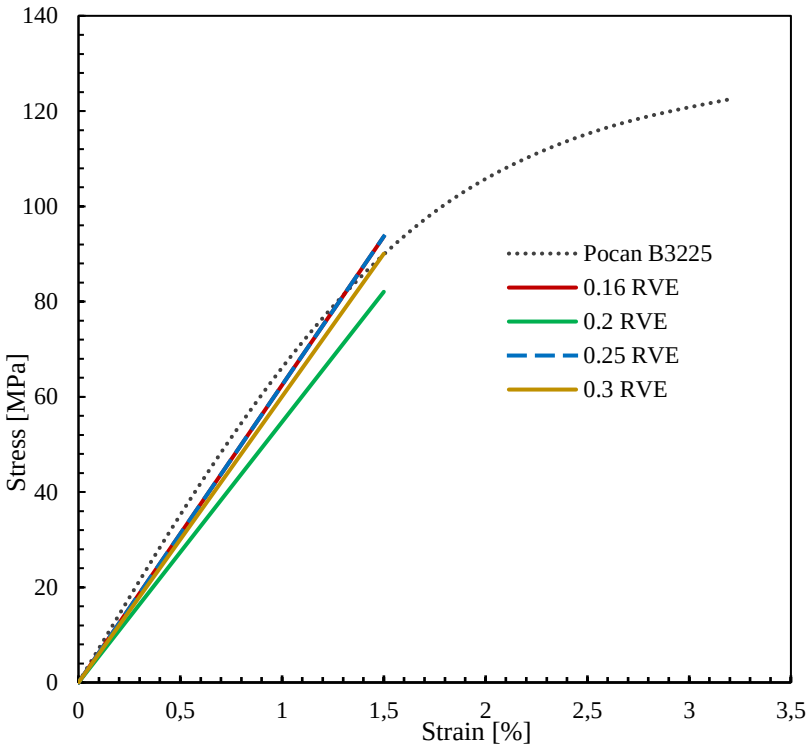

Figure 4.20 Stess-strain results for 2D RVE, random fiber orientation

4.5 Finite element analysis of 3D RVE

Next step will be to conduct same analysis as in Chapter 4.4 but only on 3D RVE. All three types of fiber orientation will be considered with all four types of RVE size.

4.5.1 3D RVE, Uniaxial orientation of glass fibers analysis

Figure 4.21 and Figure 4.22 shows all four RVE sizes used in this analysis. Periodic boundary conditions and loads were used. All fibers are oriented in one direction which is same as direction of load.

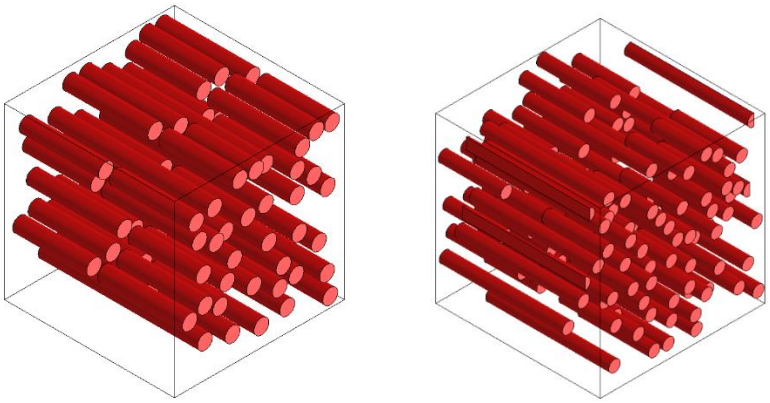

Figure 4.21 3D RVE, Uniaxial fiber orientation: 0.16 mm (left) and 0.2 mm (right)

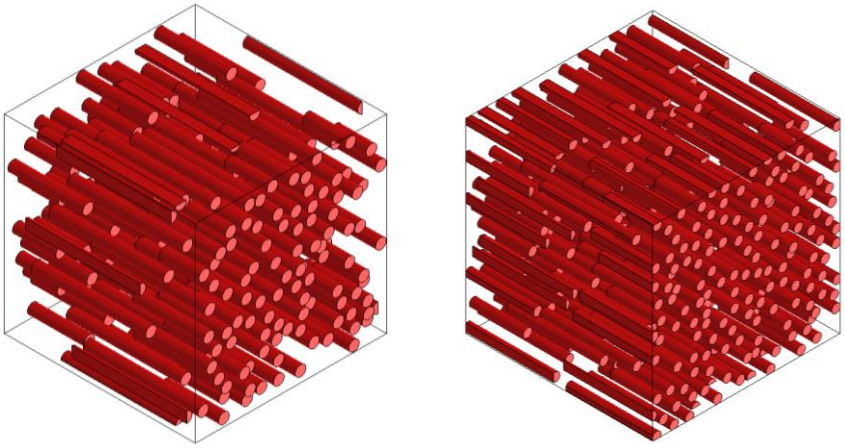

Figure 4.22 3D RVE, Uniaxial fiber orientation: 0.25 mm (left) and 0.3 mm (right)

Table 6 Inclusion number and achieved volume fraction of 3D RVE, Uniaxial fiber orientation

	1.RVE 0.16 mm	2.RVE 0.2 mm	3.RVE 0.25 mm	4.RVE 0.3 mm
Number of inclusions	36	69	135	238
Effective volume fraction [%]	0.202094	0.199157	0.199504	0.199986

Table 7 Number of finite elements per each RVE generated, 3D RVE, Uniaxial fiber orientation

	1.RVE 0.16 mm	2.RVE 0.2 mm	3.RVE 0.25 mm	4.RVE 0.3 mm
Number of C3D10M	119 762	168 198	177 803	561 404

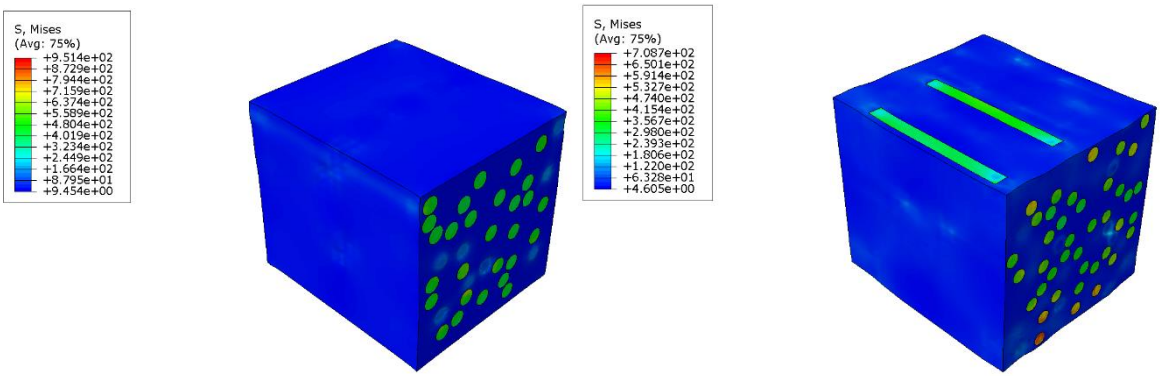

Figure 4.23 3D RVE results, Uniaxial fiber orientation: 0.16 mm (left) and 0.2 mm (right)

Table 6 and Table 7 contains information about number of inclusions, achieved volume fraction and number of finite elements that were used.

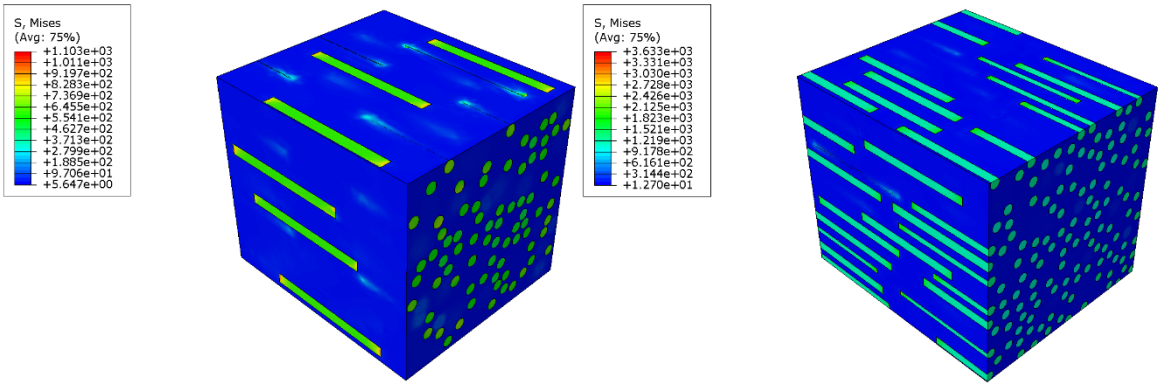

Figure 4.24 3D RVE results, Uniaxial fiber orientation: 0.25 mm (left) and 0.3 mm (right)

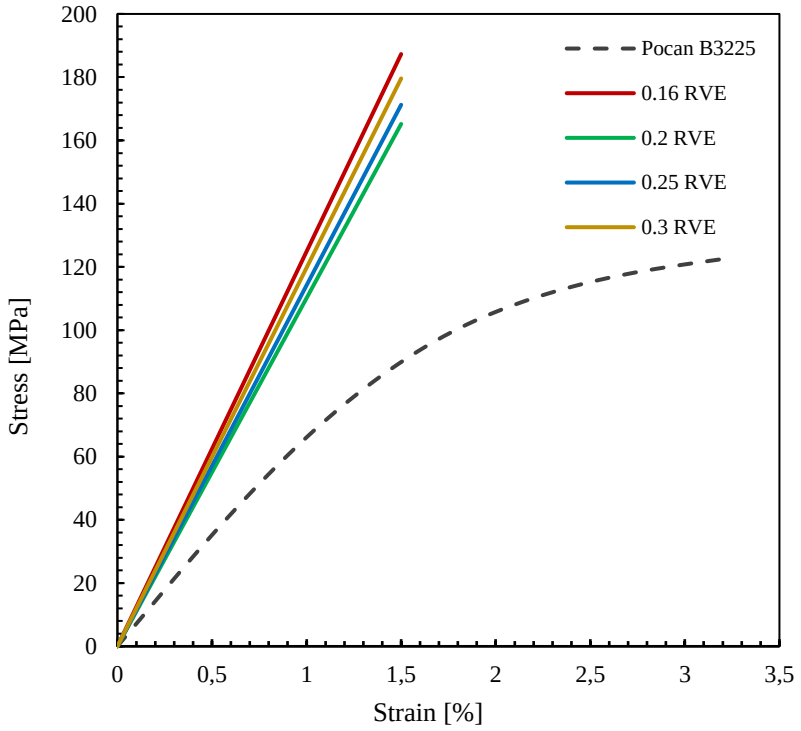

Figure 4.25 Stress-strain results for 3D RVE, Uniaxial fiber orientation

Linear-elastic results for Uniaxial fiber orientation of 3D RVE are given in Figure 4.25, and as expected stress achieved at 1.5% strain is much higher than reference Pocan B3225. Reason for higher stiffness is same as in previous cases with Uniaxial fiber orientation.

4.5.2 3D RVE, 2D random orientation of glass fibers, analysis

All input parameters are same as in previous analysis except orientation of glass fibers. Orientation is "2D random" which means that all fibers are located in planes that are mutually parallel and inside each of the planes, fibers are randomly oriented. On Figure 4.26 and Figure 4.27 are showing geometries used.

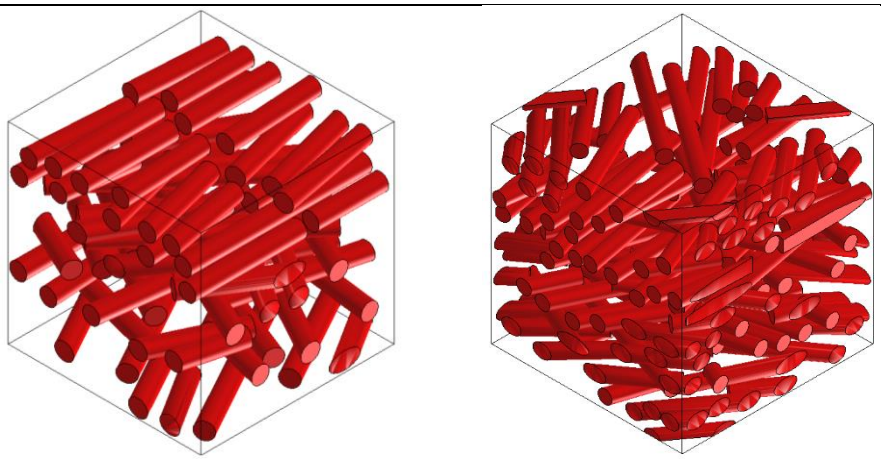

Figure 4.26 3D RVE, 2D random fiber orientation: 0.16 mm (left) and 0.2 mm (right)

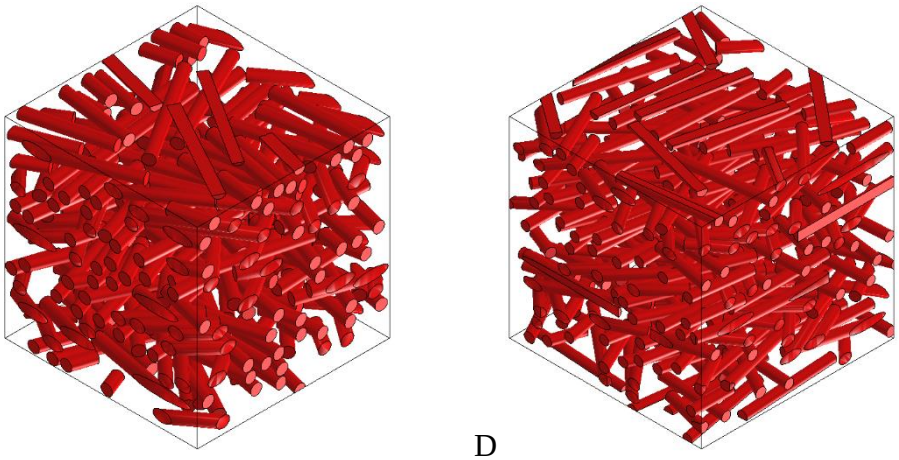

D

Figure 4.27 3D RVE, 2D random fiber orientation: 0.25 mm (left) and 0.3 mm (right)

Table 8 and Table 9 contains basic information of inclusions and mesh used.

Table 8 Inclusion number and achieved volume fraction of 3D RVE, 2D random fiber orientation

	1.RVE 0.16 mm	2.RVE 0.2 mm	3.RVE 0.25 mm	4.RVE 0.3 mm
Number of inclusions	36	69	134	234
Effective volume fraction [%]	0.202925	0.199147	0.196539	0.195838

Table 9 Number of finite elements per each RVE generated, 3D RVE, Uniaxial fiber orientation

	1.RVE 0.16 mm	2.RVE 0.2 mm	3.RVE 0.25 mm	4.RVE 0.3 mm
Number of C3D10M	100 159	150 303	307 258	307 728

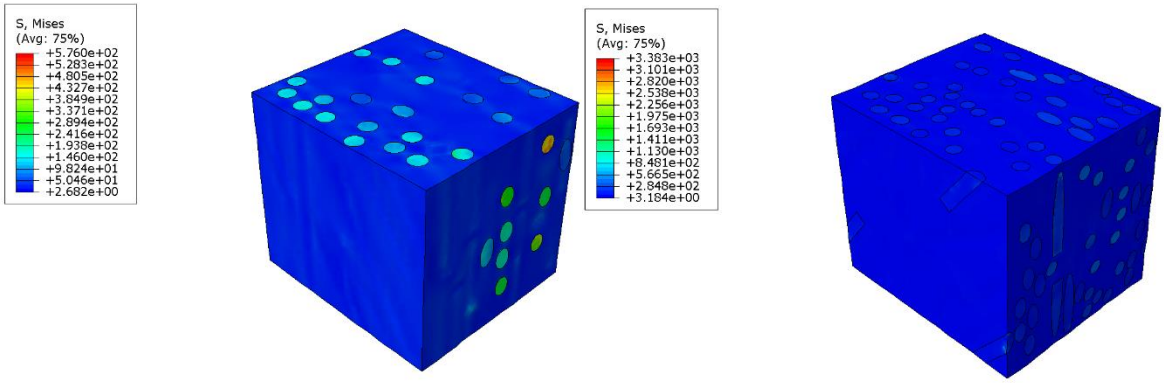

Figure 4.28 3D RVE results, 2D random fiber orientation: 0.16 mm (left) and 0.2 mm (right)

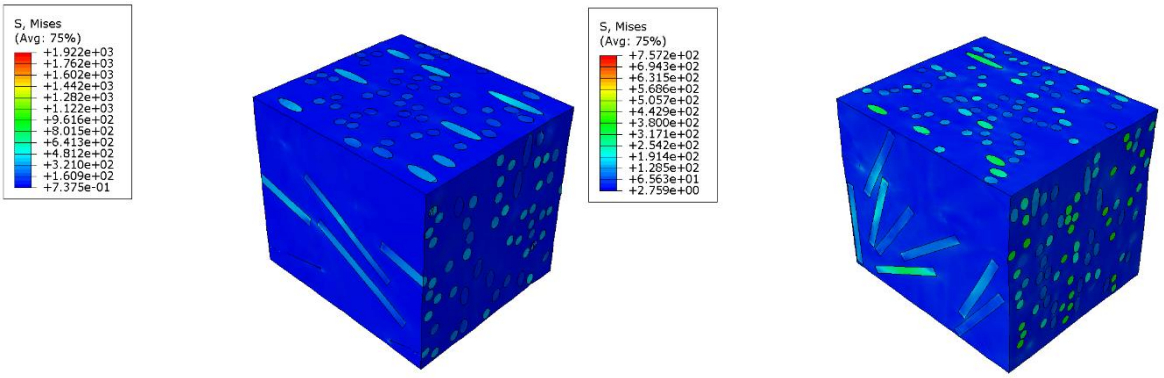

Figure 4.29 3D RVE results, 2D random fiber orientation: 0.25 mm (left) and 0.3 mm (right)

Figure 4.28 and Figure 4.29 shows analysis results with von Mises equivalent stress shown in legend. Stress-strain results were plotted and shown in Figure 4.30. 0.16 and 0.25 RVE gave lower stress results for given strain, but with 0.25 RVE linear elastic domain was well described. Conclusion is that "2D random" fiber orientation RVE model can be used well to describe macro-level with given material. Furthermore, 0.25 RVE already did good approximation of linear-elastic domain of stress-strain curve and 0.3 RVE approximately gave same results.

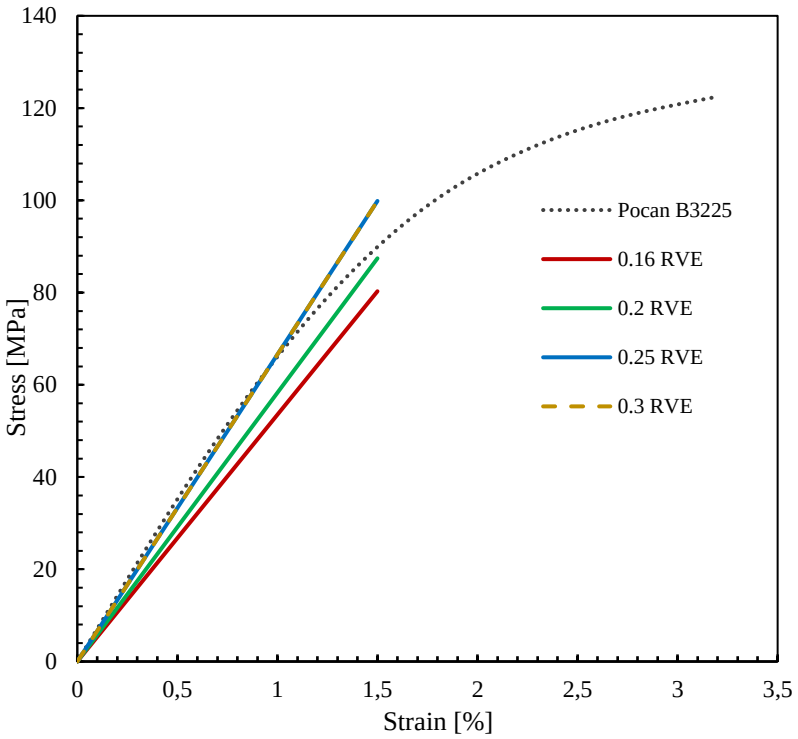

Figure 4.30 Stress-strain results for 3D RVE, 2D random fiber orientation

4.5.3 3D RVE, 3D random orientation of glass fibers analysis

Last fiber orientation to validate is 3D random. Fibers are randomly oriented in all directions inside RVE. Figure 4.31 and Figure 4.32 shows geometries that were generated and used for 3D random analysis. All others steps are same as previous cases.

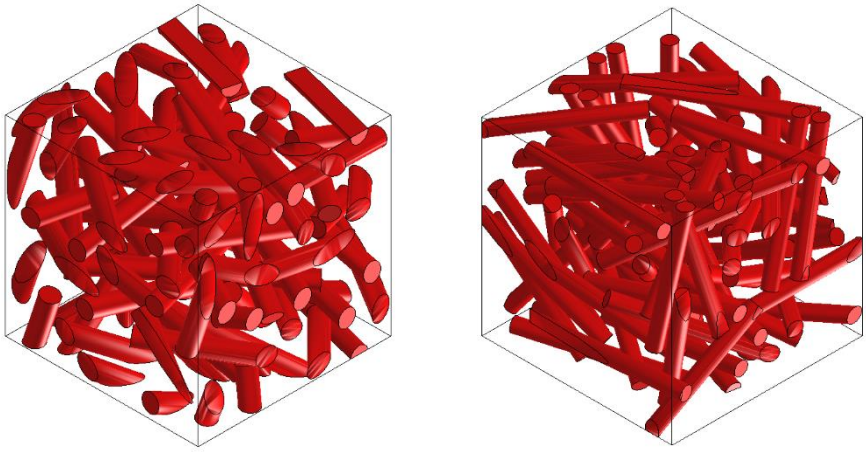

Figure 4.31 3D RVE, 3D random fiber orientation: 0.16 mm (left) and 0.2 mm (right)

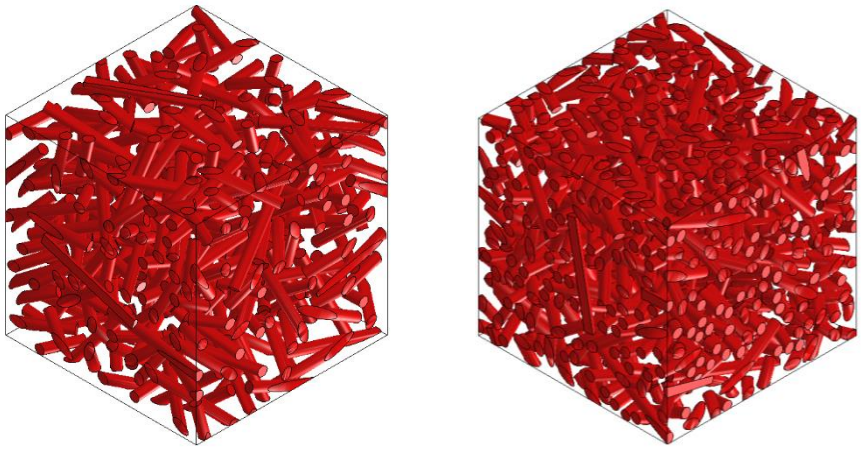

Figure 4.32 3D RVE, 3D random fiber orientation: 0.25 mm (left) and 0.3 mm (right)

Table 10 Inclusion number and achieved volume fraction of 3D RVE, 2D random fiber orientation

	1.RVE 0.16 mm	2.RVE 0.2 mm	3.RVE 0.25 mm	4.RVE 0.3 mm
Number of inclusions	36	69	135	239
Effective volume fraction [%]	0.197327	0.199381	0.200317	0.19529

Table 10 Table 11 shows general information about inclusions and mesh used in analysis.

Table 11 Number of finite elements per each RVE generated, 3D RVE, Uniaxial fiber orientation

	1.RVE 0.16 mm	2.RVE 0.2 mm	3.RVE 0.25 mm	4.RVE 0.3 mm
Number of C3D10M	123 223	196 160	273 770	561 404

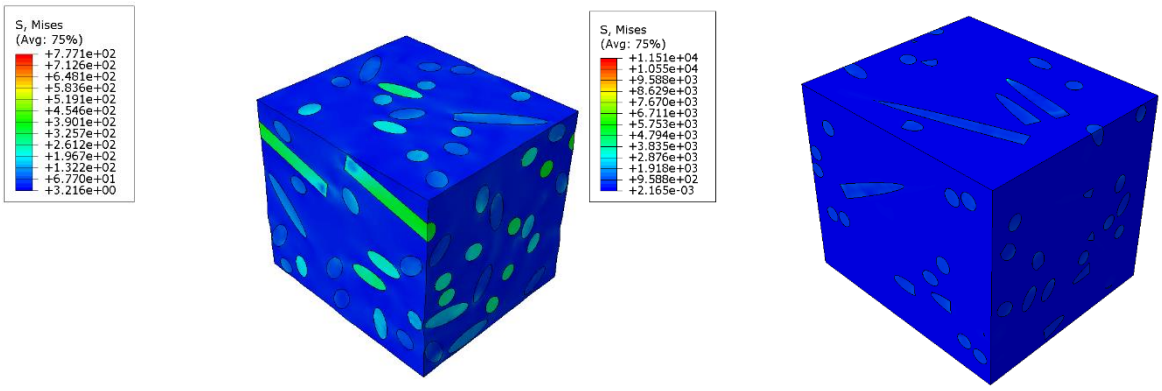

Figure 4.33 3D RVE results, 3D random fiber orientation: 0.16 mm (left) and 0.2 mm (right)

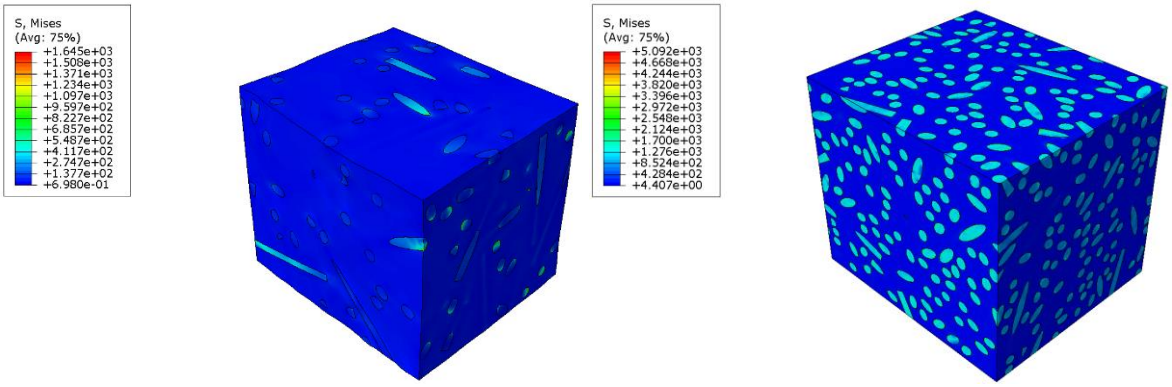

Figure 4.34 3D RVE results, 3D random fiber orientation: 0.25 mm (left) and 0.3 mm (right)

Figure 4.34 and Figure 4.35 shows results representing von Mises equivalent stress. Figure 4.35 shows volumetric mean results of linear elastic stress-strain values compared with Lanxess Pocan B3225. It is possible to conclude that 3D RVE with 3D random fibers orientations can well describe linear-elastic domain of Pocan B3225. Only 0.16 RVE showed lover values of stress-strain compared to 0.2 RVE, 0.25 RVE and 0.3 RVE.

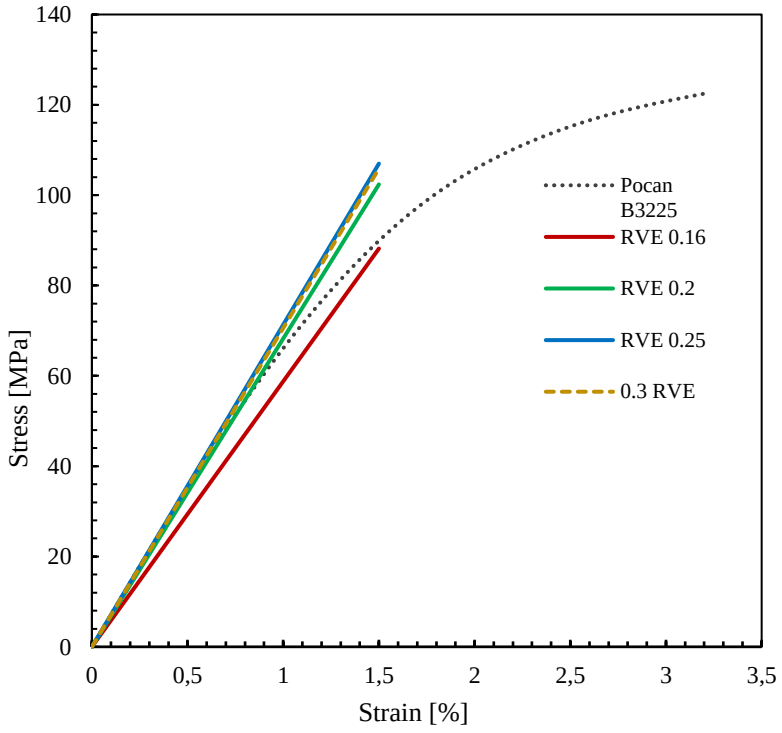

Figure 4.35 Stress-strain results for 3D RVE, 3D random fiber orientation

5 FEA of PBT with 20% GF and porosity

Following the analysis in the previous chapter, which showed that it is possible to describe the macro-level behavior of materials, depending on the orientation of the glass fibers, by using RVE, an analysis will be conducted in which, in addition to GF, voids will be added. Voids represent the porosity that occurs inside the material during injection molding. The geometry will also be generated through the *Digimat*-FE tool. Unlike the previous chapter, no analyzes will be conducted to find an RVE that does not change the result and describes the actual behavior of the material, but optimal combination of RVE and orientation of GF, will be chosen. Based on the results from the previous chapter, a 3D RVE with size of 0.25 and with a 2D random orientation GF was selected since it has been shown that it is possible to describe well the actual behavior of the material at the macro level. The goal is to match the average RVE values with the actual stress-strain values. The modeling will be performed in the same way as in the previous chapter.

In order to compare the results with the actual values, it was necessary to make test specimens containing voids. The specimens were all made with injection molding technology. The specimens were moulded from Lanxess B3225 with the addition of Hydrocerol. Hydrocerol was added to the mixture during injection as its role would be to create internal voids. After injection, the specimens were sent to CT-a scan (Computer Tomography), in order to obtain the internal void values that were required for proper modeling within the *Digimat*-FE tool. The required values are the pore size and their volume fraction in the total volume. Considering the formation of pores of different shapes during the injection, it was decided to consider the pores as spheres. Also, the pores are of different sizes and it was decided that only their average size would be considered. Figure 5.1 shows ISO 527 specimens made for experiment.

Figure 5.1 Tensile specimen ISO 527 1A

After completion of the CT scan, the specimens needed to be examined with Tensile test in order to obtain the required strain-strain values. In addition to tensile testing, the DIC (Digital

Image Correlation) method was performed. Comparison of RVE will be conducted with the results obtained by the DIC method.

The mixture that is injected into the melt when injected is Hydrocerol. Its volume content in the mixture was 0.5% and 1%. “Hydrocerol is type of blowing agents commonly used either alone or in combination with other substances to produce cellular structure in plastic mass. Hydrocerol is made out of primary chemical and activation system chemical. Primary chemical is blowing agent comprising sodium borohydride and activation system is made of sodium bicarbonate/citric acid mix which are together dispersed into polymer resin to form a mixture. the sodium borohydride and the sodium bicarbonate/citric acid mix are each encapsulated with a carrier resin to form pellets. A chemical blowing agent mixture of the sodium borohydride pellets and the sodium bicarbonate/citric acid mix pellets is then prepared. The pellets of this chemical blowing agent mixture are then fed to an injection molding machine along with the polymer resin to be foamed. The polymer resin is melted as it is fed into the barrel of the molding machine and is mixed with the chemical blowing agent mixture pellets. The heating of mixture results in the sodium bicarbonate reacting with the citric acid to release water. The sodium borohydride, in turn, reacts with water produced as a result of reaction of the sodium bicarbonate and citric acid to produce hydrogen gas. Results of such chemical reactions, blowing agents mixture is converted into gas, i.e., carbon dioxide.” [25]

After successful moulding of specimen that has volume of 1% Hydrocerol, next step is to find out what percentage of converted gas volume is in total volume of specimen. Those gas voids are representing material porosity inside material. Technology used for such purpose is Computed Tomography (CT). “CT belongs to “Non destructive testing-NDT” methods used for inspections of part without destroying it. The goal of this methods is to analyze the integrity of a material, component or structure and quantitatively measure some characteristics of the product in many different industrial applications. Due to two main advantages with respect to destructive methods (being less expensive and less time consuming) they are widely applied methods in the industrial environment. CT is tool capable of inspecting external and internal structures in many industrial applications as well as providing accurate geometrical information with very high accuracy.” [26].

In general CT system is usually made of X-ray source, rotary table, X-ray detector and data processing unit for computation, visualization and data analysis of measurement results. Figure 5.2. “In principle, CT creates cross section images by projecting a beam of emitted photons through one plane of an object from defined angle positions performing one revolution.

As the X-rays (emitted photons) pass through the object, some of them are absorbed, some are scattered, and some are transmitted. The process of X-ray intensity reduction, involving just those X-rays which are scattered or absorbed, is called attenuation. X-rays which are attenuated due to the interactions with the object do not reach the X-ray detector. Photons transmitted through the object at each angle are collected on the detector and visualized by computer, creating a complete reconstruction of the scanned object." [26] There are two main CT systems which can be found in the industry and they are 2D-CT system and 3D-CT system. In the process of making this paper, 3D-cT system was used.

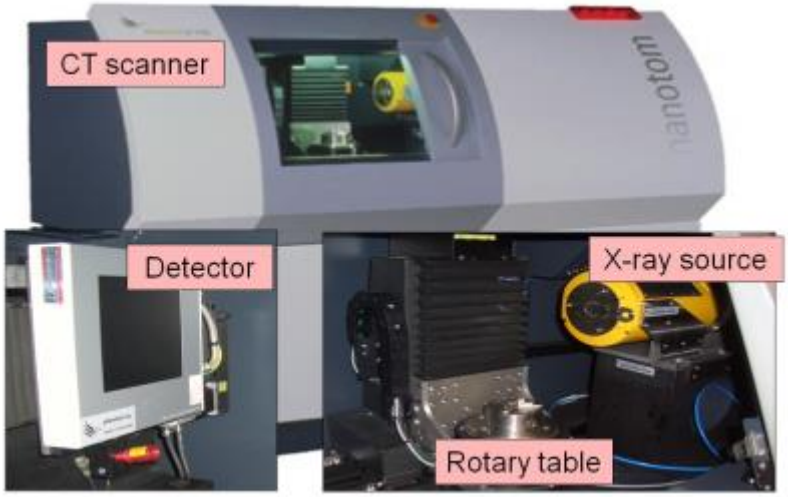

Figure 5.2 Industrial cone beam CT scanner [26]

The 3D-CT system consists of a flat area detector and a cone beam source, enabling the acquisition of a slide of the object just with one revolution of the rotary table, which is shown on Figure 5.3. No linear translation of the rotary table is needed. This solution allows significant improvement in acquisition time.

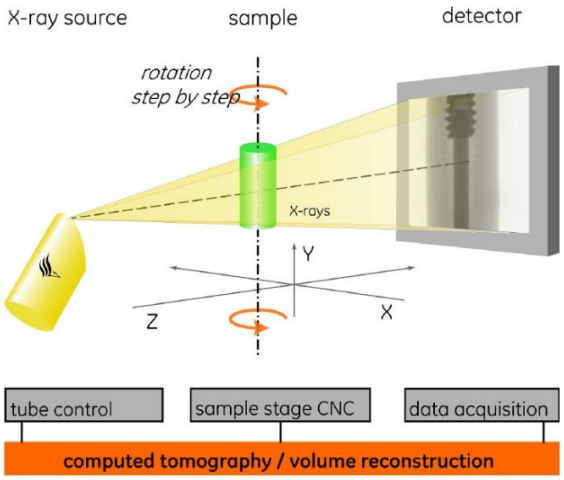

Figure 5.3 3D-CT with flat panel detector

Digital Image Correlation (DIC) is method used for measuring surface displacement. The displacement components on the surface of an object are easily obtained using this method by recording the images of surface before and after deformation. The plane surface of an object is observed by a CCD camera with an imaging lens.

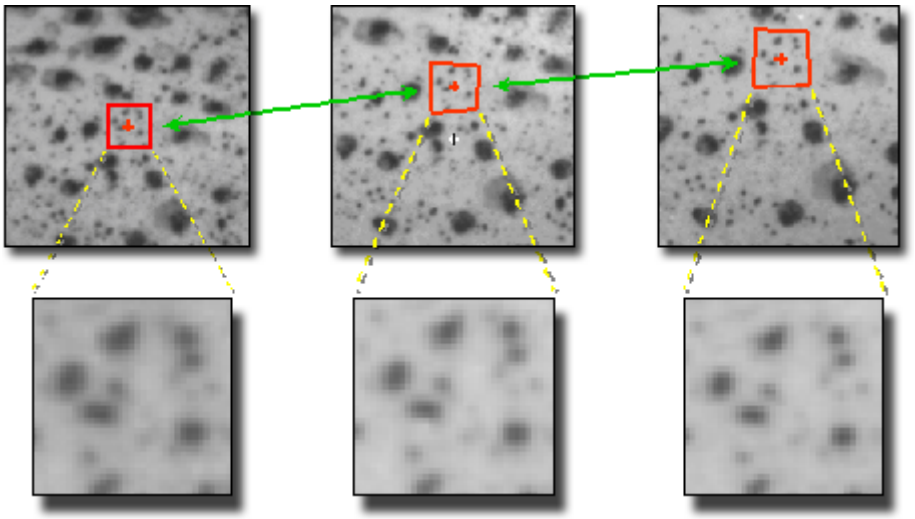

Figure 5.4 Matching the subset before and after deformation [27]

Then, the images on the surface of the object, one before and another after deformation, are recorded, digitized and stored in a computer as digital images." These images are compared to detect displacements to find matched point from one image to another. The displacement of analyzed subset on the image before deformation is found in the image after deformation by searching the area of the same light intensity distribution with the subset. Once the location of this subset in the deformed image is found, the displacement of this subset can be determined. In order to perform this process, the surface of the object must have a feature that allows matching the subset. If no feature is observed on the surface of the object, an artificial random pattern must be applied." [28] On Figure 5.6 is shown pattern that was applied on specimens used in this thesis.

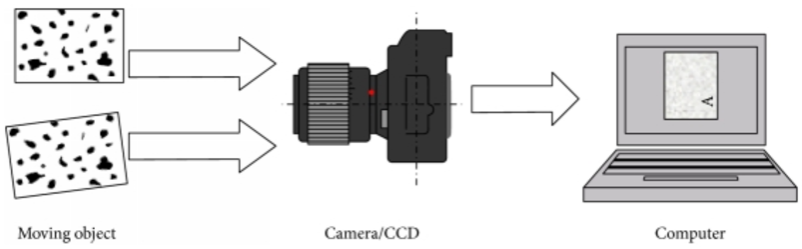

Figure 5.5 Setup for displacement measurement using digital image correlation (DIC) [29]

In order to conduct tensile test and measure displacement with Digital Image Correlation, random pattern was applied on specimens as shown on Figure 5.6. Tensile test was then conducted while measuring displacement by Digital Image Correlation (DIC).

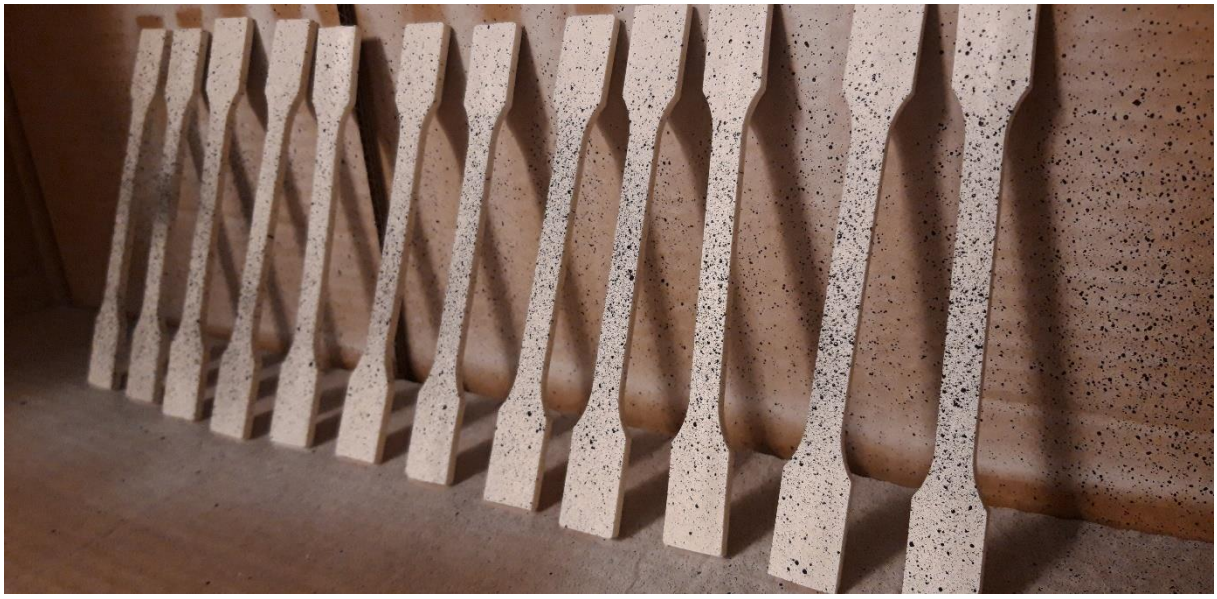

Figure 5.6 Specimens (ISO 527) with applied random pattern for DIC

Tensile test was conducted while measuring displacement with Digital Image Correlation (DIC).

Figure 5.7 Specimen subjected to tensile test while also measured with DIC

Closer view of specimen and rupture is shown on Figure 5.8.

Figure 5.8 View of specimen before (up) and after (down) the rupture

Finally, after the tensile test and all data collected, analysis same as in Chapter 4.3 can be conducted. As said, in this chapter analysis will be conducted on PBT containing 20% glass fibers, but now with pores. Pores are modeled as perfect spheres, in order to make easier model to mesh and generate. Furthermore, actual pores don't have regular geometry which can be big problem to model such geometry. That is also a reason why spherical geometry of pores was taken. Pores will be randomly placed inside RVE and generated model will be consisted of 0.25 RVE with 2D random orientation of glass fibers. Figure 5.9 shows results of the experiment on specimens with 0.5% and 1% Hydrocerol mixture inside material. Experimental stress-strain results are compared with basic Pocan B3225.

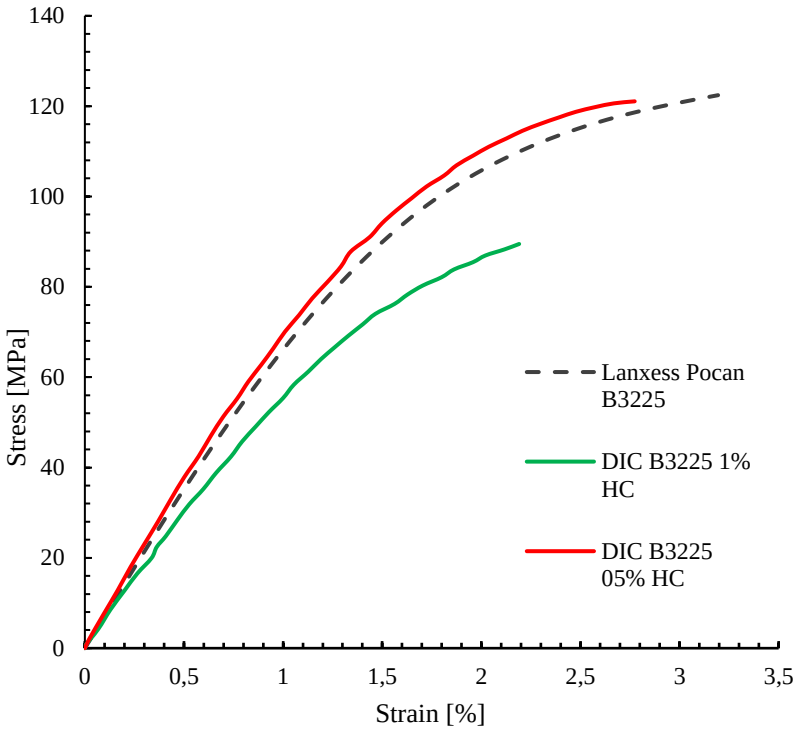

Figure 5.9 Experimental results of B3225 with 0.5% HC and 1% HC compared to basic B3225

5.1 FEA of B3225 with 1% HC

Analysis will be conducted only on B3225 with 1% HC. In order to get correct information about pores inside material, CT was used. Statistical results from CT are given in Table 12.

Table 12 CT results for B3225 with 1% HC

B3225; 1% HC	
V_{min} [mm^3]	0,001
V_{max} [mm^3]	0,0038
V_{mean} [mm^3]	0,3595
Void fraction [%]	1.90

In order to model sphere geometry in *Digimat*-FE tool, diameter of void is needed. From value of mean volume of void diameter can be calculated and diameter equals 0.19 mm. Void with diameter of 0.19 mm can hardly fit in RVE of 0.25 mm. Even RVE of 0.3 mm wouldn't help because fitting such void in, will lead to inability to fill volume fraction of 20 % of GF. Figure 5.10 shows what it looks like when such inclusion sphere is fitted inside 0.25 RVE. Trying to analyze RVE bigger even from 0.3 mm, will probably solve problem of fitting such big sphere in but other problems will occur. Because void inclusion is so big relative to glass fibers, bigger RVE will contain hundreds of GF more, and such models are too difficult to mesh and analyze.

The way in which the analysis will be conducted is as follows. The volume fraction of voids will not change but the number of pores within the RVE will change, meaning that the average pore size will be ignored since it is impossible to model it this way. 4 models will be considered and each will have a different pore number but with an equal volume fraction of all pores in RVE.

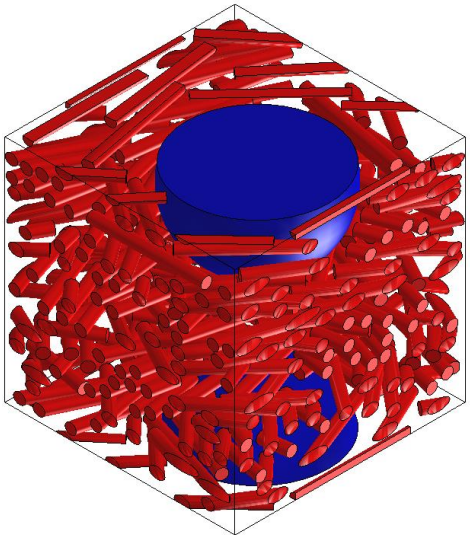

Figure 5.10 0.25 RVE with one inclusion sphere of 0.19 in diameter

Basic information's about RVEs used are given in Table 13.

Table 13 Basic information about RVE's used in void analysis

B3225 with 1% HC	RVE 1	RVE 2	RVE 3	RVE 4
Number of void inclusions	1	3	10	20
Number of GF inclusions	136	135	135	136
Targeted volume fraction of pores	1.9%			
Achieved volume fraction of pores	1.9%	1.9%	1.86689%	1.89789%
Number of FE	278 131	293 876	300 655	328 127

Procedure of conducting the analysis is same as in Chapter 5, which means that any RVE model will be generated inside *Digimat*-FE tool and FEA will be conducted with software package Abaqus. Mean stress-strain results will be then plotted with B3225 1% HC. Figure 5.11 and Figure 5.12 shows geometries with voids that were used in this chapter.

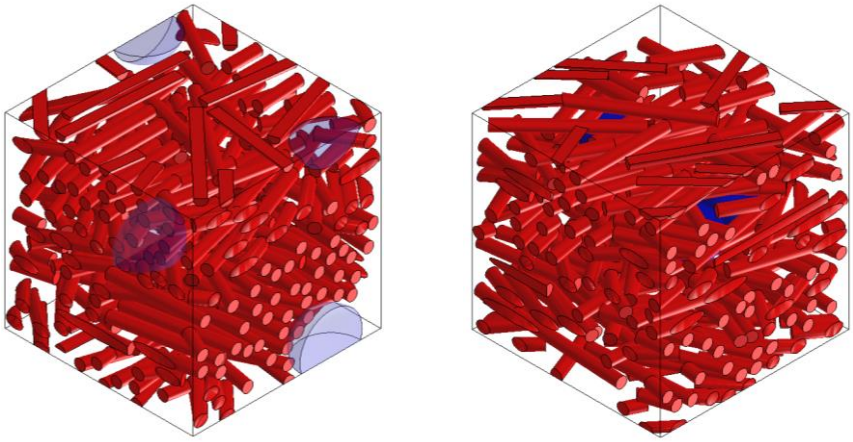

Figure 5.11 0.25 RVE geometries with 1 void (left) and 3 voids (right)

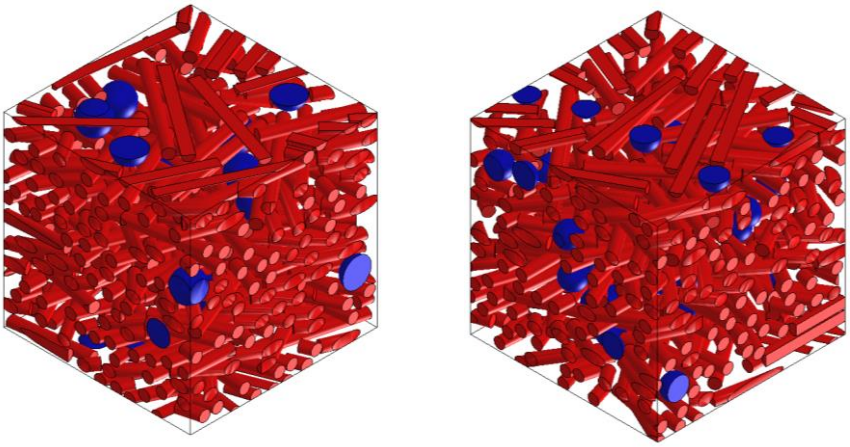

Figure 5.12 0.25 RVE geometries with 10 void (left) and 20 voids (right)

Results with von Mises equivalent stress shown, are given in Figure 5.13 and Figure 5.14.

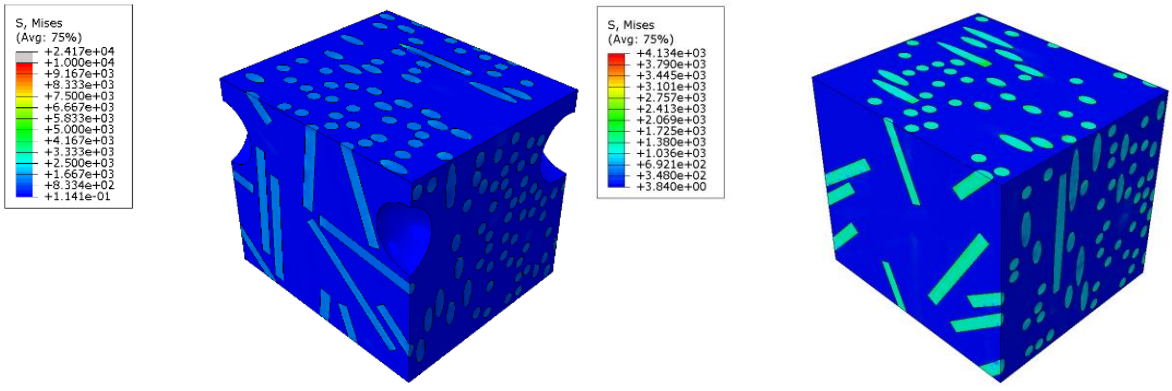

Figure 5.13 0.25 RVE geometries with 1 void (left) and 3 voids (right)

Finally, mean stress-strain results are plotted and compared with B3225 1% HC in Figure 5.15.

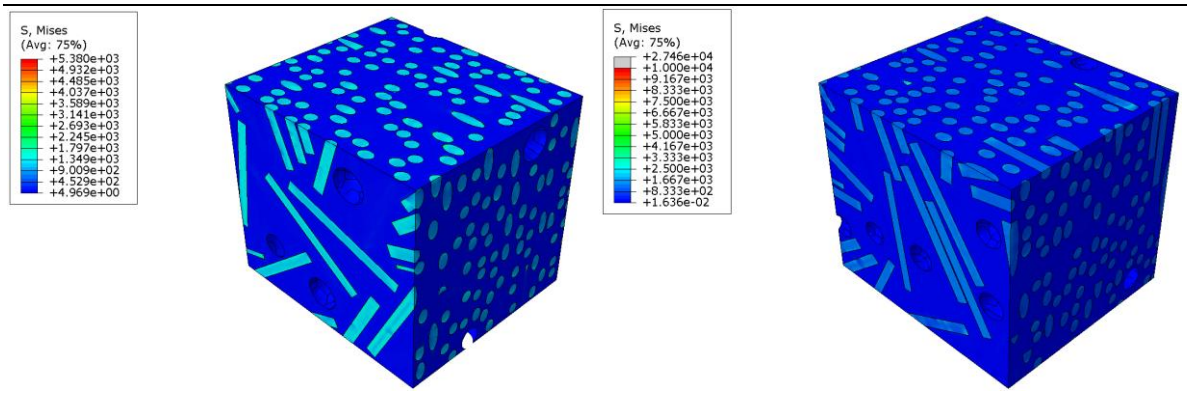

Figure 5.14 Results of 0.25 RVE geometries with 10 void (left) and 20 voids (right)

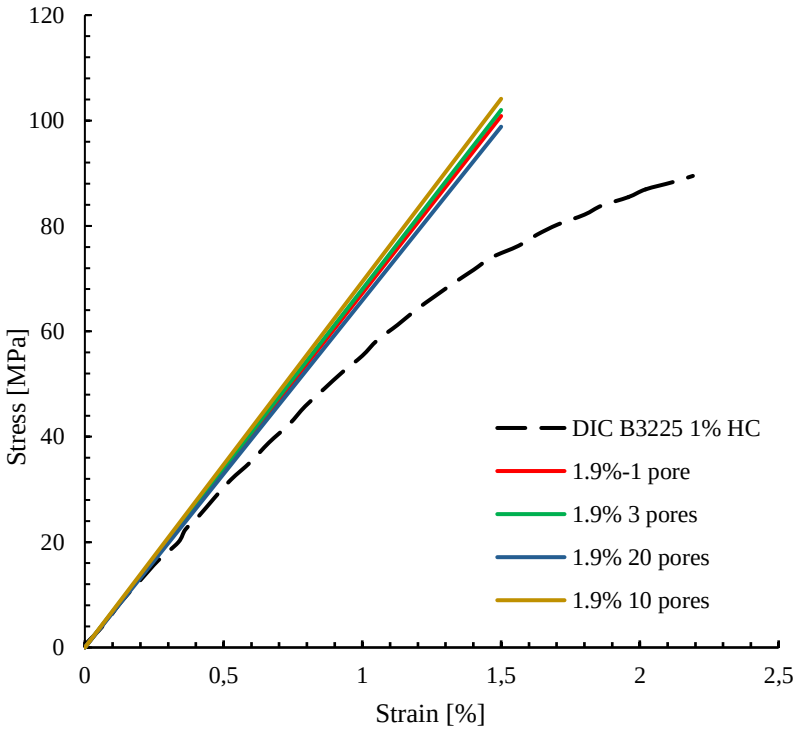

Figure 5.15 Stress-strain results compared with B3225 1% HC

The results obtained and shown in Figure 5.15 give more rigidity to material than the results of the experiment. The reasons why this is so can be various. Several assumptions were made in the modeling that probably led to these results. The first is that the geometry of the pores was considered as a perfect sphere even though it is not in reality. Also, with the resulting mean pore size, 0.25 and 0.3 RVE is simply too small and if RVE is made bigger, serious problems with meshing and hardware capacities will occur. The last assumption is that it is possible to change or reduce the pore size with the unchanged pore volume in the material-

6 Conclusion

Main objectives of this this are as follows:

1. To determine the necessary 2D and 3D RVE consisting of PBT with glass fibers (GF) while using homogenization methodology
2. To expand model with PBT and GF with porosity
3. To validate numerical results with experimental measurement.

After initial studying of anisotropic material behavior and homogenization methods, steps were performed on 2D and 3D RVE linear-elastic analyzes. Model generations was made in *Digimat*-FE and *Digimat*-MF tool, given whether it was used mean-field homogenization method or finite element analysis. First step was to validate 2D RVE numerical results with Pocan B3225. Uniaxial fiber orientation showed much higher rigidity, as expected, because given loads and boundary conditions were in same axes as all of fibers oriented. Random fiber orientation gave much closer results than uniaxial. Same procedure was done on 3D RVE. Three different fiber orientation was analyzed, each having 4 different sizes of RVE. In all cases third RVE already gave results after which there were no major changes. Uniaxial fiber orientation in 3D also gave more rigid results while comparing with Pocan B3225. Also, 2D random and 3D random fiber orientations models gave approximately same results compared to B3225. Only difference was that 3D RVE with 2D random fiber orientation is much easier to generate and mesh. In last step goal was to model appearance of porosity inside base material Pocan B3225. In order to get geometrical inputs to model such pores, test specimens were made with extra mixture of Hydrocerol (HC). HC was added and trapped inside, which caused occurrence of voids (pores) inside the material. Those specimens with pores was subjected to tensile test, in order to get stress-strain curves for experimental validation of numerical results. Porosity was modeled on 0.25 RVE model with 2D random fiber orientation because that model showed good results match and it didn’t require large hardware needs. After conducted analysis, results were compared with stress-strain curves of experimental results and linear elastic domain was not well approximated and reason may be in false assumptions that are described in thesis.

There are some recommendations for future work. The idea of trying to model fixed volume fraction of pores, but with different number of inclusions, should be analyzed more in detail. Reason why this can be useful is because on micro levels there can be two or more phases whose dimensions can be very different. That is the case in this thesis, mean dimension of spheres are so much larger that closes representative volume element would have a few

hundreds, glass fibers inclusions, more than biggest RVE analyzed in this this. This relative distinction in geometries can cause much problems in analysis that have two or even more phases. Next recommendation is about fiber orientations. In whole thesis, fiber orientations were modeled and compared with results of Pocan B3225 whose glass fiber orientation are unknown. *Digimat* even have option to import orientations of inclusion from plastic injection molding software, such as Moldflow. In order to model such RVE with much closer fiber orientation, it is possible to conduct some research in this direction.

Bibliography

[1] "Polybutylene-terphthalate." [Online]. Available: https://www.britannica.com/science/polybutylene-terephthalate.

[2] "Polybutilene terephthalate, Figure." [Online]. Available: https://en.wikipedia.org/wiki/Polybutylene_terephthalate.

[3] "Pocan B3225." [Online]. Available: https://www.campusplastics.com/campus/en/datasheet/Pocan+B3225+000000/LANXESS+Deutschland+GmbH/99/9d2ca065.

[4] "Pocan B1305 000000." [Online]. Available: https://www.campusplastics.com/campus/en/datasheet/Pocan+B1305+000000/LANXESS/99/a5c1c937/SI?pos=0.

[5] "Pocan B1305 000000." [Online]. Available: https://www.materialdatacenter.com/ms/en/Pocan/LANXESS+Deutschland+GmbH/Pocan+B1305+000000/a5c1c937/1455.

[6] R. G. Kleijnen, J. P. W. Sesseg, M. Schmid, and K. Wegener, "Insights into the development of a short-fiber reinforced polypropylene for laser sintering," *AIP Conf. Proc.*, vol. 1914, no. December, 2017.

[7] "GF Poisson's factor." [Online]. Available: https://www.azom.com/properties.aspx?ArticleID=764.

[8] D. Siminiati, L. Pomeni, and Ć. F. Orši, "THE BASE PARAMETER ADJUSTMENT FOR INJECTION MOULDING," vol. 1, pp. 119–127, 2008.

[9] L. Corporation, "Part and Mold Design." p. 168, 2007.

[10] K. Volokh and K. Volokh, "Anisotropic Elasticity," *Mech. Soft Mater.*, pp. 77–90, 2016.

[11] *Digimat manual, Release 5.1.1 - August 2014*, no. August. 2014.

[12] I. Doghri and A. Ouaar, "Homogenization of two-phase elasto-plastic composite materials and structures study of tangent operators, cyclic plasticity and numerical algorithms," *Int. J. Solids Struct.*, vol. 40, no. 7, pp. 1681–1712, 2003.

[13] L. Brassart, I. Doghri, and L. Delannay, "Homogenization of elasto-plastic composites coupled with a nonlinear finite element analysis of the equivalent inclusion problem," *Int. J. Solids Struct.*, vol. 47, no. 5, pp. 716–729, 2010.

[14] J. D. Eshelby, “The determination of the elastic filed of an ellipsoidal inclusion and related problems,” *Proceeding R. Socitey*, 1957.

[15] Z. Hashin and S. Shtrikman, “A variational approach to the theory of the elastic behaviour of multiphase materials,” *J. Mech. Phys. Solids*, vol. 11, no. 2, pp. 127–140, Mar. 1963.

[16] Y. Benveniste, “A new approach to the application of Mori-Tanaka’s theory in composite materials,” *Mech. Mater.*, vol. 6, no. 2, pp. 147–157, 1987.

[17] “DIGIMAT.” E-Xstream Engineering, Hautcharage Luxemburg, 2014.

[18] O. C. ZIENKIEWICZ, *The finite element method.* London: McGraw-Hill, 1977.

[19] O. C. Zienkiewicz and R. L. Taylor, *The finite element method. Volume 1: Basic formulation and linear problems*. 1994.

[20] J. SORIĆ, *Metoda konačnih elemenata*. Zagreb: Golden marketing - Tehnička knjiga, 2004.

[21] “Finite element method.” [Online]. Available: http://www.studioseed.net/research/estructuras/calculo-dinamico/what-does-shape-function-mean-in-finite-element-formulation/.

[22] O. C. Zienkiewicz, R. L. Taylor, and J. Z. Zhu, “The Finite Element Method: Its Basis and Fundamentals,” *Int. J. Numer. Methods Eng.*, p. 733, 2005.

[23] “C3D10 and C3D10M elements.” [Online]. Available: http://optimec.ca/news/tetrahedral-elements-available-abaqus-structural-analysis-use/.

[24] “ABAQUS, 6.14-5.” .

[25] “US4769397.” .

[26] “Introduction_to_CT.pdf.” .

[27] “Digital Image Correlation (DIC).” [Online]. Available: https://www.correlatedsolutions.com/digital-image-correlation/.

[28] S. Yoneyama and G. Murasawa, “Digital Image Correlation, in Experimental Mechanics,” *Encycl. Life Support Syst.*, pp. 1–10, 2009.

[29] M. H. Shih and W. P. Sung, “Developing dynamic digital image correlation technique to monitor structural damage of old buildings under external excitation,” *Shock Vib.*, vol. 2014, no. July, 2014.